Hydrogen-rich gas production by steam reforming of n-dodecane.

Part I: Catalytic activity of Pt/CeO_2 catalysts in optimized bed configuration

Antonio Vita, Cristina Italiano, Concetto Fabiano, Lidia Pino, Massimo Laganà and Vincenzo Recupero

CNR-ITAE "Nicola Giordano", Via Salita S. Lucia sopra Contesse 5, 98126 Messina – Italy

*Corresponding author: antonio.vita@itae.cnr.it, Phone:+39090624297

Abstract

Onboard diesel reformer integrated with solid oxide fuel cell (SOFC) unit offers potential for high energy conversion efficiency and low emission levels on seagoing transport, avoiding cost associated with hydrogen storage and infrastructure. However, the development of active and stable liquid hydrocarbon-reforming catalyst still remains one of the major technological barriers for fuel-cell-based auxiliary power unit (APU) applications.

In this paper, the activity and stability of Pt/CeO_2 catalysts were investigated towards the steam reforming (SR) of n-dodecane, used as surrogate fuel for marine diesel. Pt-based catalysts (0.6-2.3 wt.% of metal loading) were prepared by Solution Combustion Synthesis (SCS) method and characterized by XRD, N_2-physisorption, CO-chemisorption, TPR, TPO and TEM techniques. Tests were performed at various process parameters, namely steam-to-carbon molar ratio (S/C=2-3), space velocity (GHSV=16,000-32,000 h^{-1}) and time-on-stream. An optimized temperature-controlled (500-800°C) bed configuration was adopted in order to avoid carbon/coke deposition due to n-dodecane cracking phenomena.

Superior chemical-physical properties of 0.6 wt.% Pt/CeO_2 system positively affect the SR performance. Pt-based catalyst showed catalytic activity comparable with that of the commercial Rh/ZDC (Rh/Zirconia-doped-Ceria). Total n-dodecane conversion and high H_2 concentration (73%, dry and N_2-free basis) were obtained at S/C=2.5 and GHSV=16,000 h^{-1}. Stable catalytic activity was found under start-up and shut-down cycles for 50 hours of time-on-stream. Restored catalytic performance was obtained under activity-regeneration cycles evaluated in more stressful conditions (S/C=1.5; GHSV=40,000 h^{-1}). This preliminary study was finalized to a diesel fuel processor design.

Keywords: hydrogen, diesel, n-dodecane, platinum-ceria catalyst, steam reforming.

1. Introduction

Energy generation in fuel cell (FC)-based auxiliary power units (APUs) is a very desirable option for both pollutants reduction and efficiency improvement in the transport sector [1,2]; the APU device, consisting of a fuel reformer, a cleanup system for reformate and a fuel cell stack, can provide energy for functions other than propulsion. APUs take advantage of liquid hydrocarbons (gasoline, diesel, kerosene) due to the easier storage and transportation compared to hydrogen, which is produced onboard; fuel cells used in APU systems include molten carbonate fuel cells (MCFCs), solid oxide fuel cells (SOFCs) and proton exchange membrane fuel cells (PEMFCs) [3]. The high temperature operation of SOFCs has the advantage of fuel flexibility: light hydrocarbons and CO can be used as fuels, avoiding the purification step (water gas shift and preferential oxidation or pressure swing adsorption) to obtain high purity hydrogen from syngas mixture [4]. SOFC-based APU systems, powered by the same type of fuel (diesel) used in the principal engine, are particularly interesting alternatives for supplying electrical energy to seagoing vehicles because can generate enough power for cabin comfort, to supply electricity for the refrigeration of load [5]. Diesel is the most used feedstock due to high energy density and existing fuel infrastructure [6].

Catalytic steam reforming (SR) of diesel can be considered the most important route for high hydrogen yield and high hydrogen concentration in the effluent gas [7]. Diesel fuel is a complex mixture of hydrocarbons (alkanes, cycloalkanes and aromatics, with carbon numbers ranging between 12 to 20) and sulfur compounds (alkylbenzothiophene and alkyldibenzothiopnene) [8]. In this study, n-dodecane ($C_{12}H_{26}$) was used as model compound for diesel fuel.

The highly endothermic SR of n-dodecane reaction (Eq. 1), with the simultaneous occurrence of water gas shift (WGS, Eq. 2) reaction:

$$C_{12}H_{26} + 12H_2O \rightarrow 12CO + 25H_2, \qquad \Delta H^{\circ}_{298} = 1866.5\ kJ \cdot mol^{-1} \tag{1}$$

$$CO + H_2O \leftrightarrow CO_2 + H_2, \qquad \Delta H^{\circ}_{298} = -41.1\ kJ \cdot mol^{-1} \tag{2}$$

proceeds on the catalyst surface by sequential steps forming lighter hydrocarbons that, in turn, react with steam, forming a mixture of H_2, CO and CO_2. However, due to the complexity of high-molecular-weight hydrocarbon reforming processes, numerous chemical reactions (i.e., methanation, thermal cracking, Boudouard and gasification,) can occur [9].

Carbon and coke deposition are major problems in reforming processes of high molecular weight hydrocarbon; this represents one of the major technological barriers that prevents the implementation of on-board liquid hydrocarbon reforming technology [10,11]. Coke is produced by thermal cracking of hydrocarbons, through the sequence reported in

Eq. 3, depending on the condition in which coke was formed: amorphous (filamentous) carbon is favored at low temperatures (<600°C) while graphitic (whisker) carbon is favored at high temperatures (>600°C) [12].

$$C_{12}H_{26} \rightarrow Olefins \rightarrow Polymers \rightarrow Coke \rightarrow Amorphous\ carbon \rightarrow Graphitic\ carbon \quad (3)$$

Carbon is produced by Boudouard reaction (Eq. 4), reverse gasification (Eq. 5) and hydrocarbons decomposition. Carbon forms can vary from whisker to filamentous depending on the operating conditions: Boudouard and reverse gasification reactions are favored at low temperatures, while hydrocarbons decomposition is favored at high temperatures [10,13].

$$2CO \rightarrow C + CO_2, \qquad \Delta H^{\circ}_{298} = -86.3\ kJ \cdot mol^{-1} \quad (4)$$

$$CO + H_2 \rightarrow C + H_2O, \qquad \Delta H^{\circ}_{298} = -130.4\ kJ \cdot mol^{-1} \quad (5)$$

Carbon and coke formation could cause degradation of the reformer performance and reduce its lifetime significantly. In a reformer system, there is a potential for carbon/coke formation in the catalytic reactor (reformer) as well as in its upstream and downstream units (i.e. vaporizer unit) [14]. Thus, there are several concerns for the design and operation of a reforming system for heavy hydrocarbon fuels [15]. One of the most crucial factors that influence the reforming performance is the uniform mixing between the reactants. As reported by Hartmann et al. [16], a not homogeneous mixture can be cause of hot spots, unwanted by-products formation and consequent carbon/coke deposition. Therefore, liquid fuels such as n-dodecane can be atomized and vaporized into microscopically sized droplets, while the overall reforming efficiency significantly improves by spraying the fuel with injection nozzles [17]. Porš et al. [18] and Pasel et al. [19] demonstrated that the long-term reforming performance could be improved by spraying the liquid fuel by twin fluid or swirl nozzle. An et al. [20] used a twin fluid nozzle to facilitate uniform mixing; they reported that reforming performance increased with shorter distance from the nozzle to the catalytic bed and larger mean drop size of fuel droplets. Alternatively, Koo et al. [21] demonstrated that a pre-reforming catalyst, installed after the gas-liquid spray nozzle, minimized the risk of carbon/coke formation due to the decomposition of the fuel. Xu et al. [22] investigated the reactants' inlet temperatures in order to avoid carbon formation inside the heating hose and to enhance the conversion efficiency.

The development of active and stable catalysts remains yet one of the major technological barriers for direct liquid hydrocarbon reforming at high temperature (800°C). Noble-metal-based catalysts (Pt, Rh, Pd, Ru) are more efficient because of their long-term activity and strong resistance to carbon [23-28]; besides, the presence of organic sulfur impurities in liquid hydrocarbons can affect the carbon deposition on reforming catalysts. Rh-based catalysts show higher sulfur tolerance than Pt, Ru and Ni catalysts during reforming reaction at 800°C [29]. Analogous trend was reported by Shekhawat et al. [30] towards n-tetradecane reforming in presence of sulfur. The effect of noble metal

catalysts supported on different supports (Al_2O_3, SiO_2, CeO_2 and MgO) was examined by Song and co-workers [31] in steam reforming of sulfur-containing liquid hydrocarbons (Norpar 13, Exxon Mobil). This systematic study confirms the high sulfur tolerance of Rh/Al_2O_3 catalyst in comparison with Ru, Pt and Pd samples on the same support; both Al_2O_3 and CeO_2 appear as promising supports for Rh, while CeO_2 emerges as the most adequate support for Pt.

The role of CeO_2 as promoter and/or support in catalysts formulation, due to its oxygen storage capacity (OSC), that can improve the reversibility of oxidation/reduction reactions of noble metals and the adsorption/dissociation of steam in catalyst surface increasing coke gasification, has been widely reported [32,33]. Our group has undertaken some studies on metal-supported CeO_2 catalysts prepared by combustion synthesis [34]; the derived strong metal-to-support interaction appears strictly related to the observed high catalytic activity and stability during hydrocarbons reforming. Moreover, the combustion synthesis provides an attractive practical alternative to the conventional preparation methods since is simple, low in cost, saving in time and energy consumption [33,34].

On this basis, the current investigation focuses the activity, stability and regenerability of Pt/CeO_2 catalysts, during steam reforming (SR) of n-dodecane, used as surrogate fuel for marine diesel. This preliminary study constitutes the first step of a more complete investigation (in progress) finalized to the development of a catalytic system for a diesel fuel reformer unit [35].

The Pt-based catalysts (0.6-2.3 wt.% of metal loading), prepared by Solution Combustion Synthesis (SCS) method, were characterized by XRD, N_2-physisorption, CO-chemisorption, TPR, TPO and TEM techniques. Tests were performed at various process parameters, namely steam-to-carbon molar ratio (S/C=2-3), space velocity (GHSV=16,000-32,000 h^{-1}) and time-on-stream. Results were compared with those of a commercial catalyst based on Rh/ZDC (Rh/Zirconia doped Ceria). An optimized temperature-controlled bed configuration (500-800°C) was developed in order to avoid carbon/coke deposition due to n-dodecane cracking phenomena.

2. Experimental Section

2.1. Catalysts Synthesis

Pt/CeO_2 catalysts were prepared by the Solution Combustion Synthesis (SCS) method, according to the procedure described elsewhere [36-38]. In a typical experiment, stoichiometric amount of Ce [$Ce(NO_3)_3$ from Sigma Aldrich] and Pt [H_2PtCl_6 from Sigma Aldrich] precursors with the suitable quantity of fuel [urea, CH_4N_2O from Alfa Aesar] were dissolved in a minimum quantity of water. The amount of catalyst precursors was adjusted in order to prepare samples with different platinum content, ranging between 0.6 wt.% and 2.3 wt.%. The amount of fuel was determined by the so-called fuel-to-oxidant ratio and it was calculated using the total oxidizing (O) and reducing (F) valences of the components in order to have an equivalence ratio equal to 1 (ϕ=O/F=1), that corresponds to the maximum release of

energy. The combustion mixture, gently aged in a quartz container of 600 cm^3 capacity until a homogeneous slurry was formed, was introduced into a preheated muffle furnace (350°C). At the beginning the slurry boils, foams and then undergoes intense flaming combustion with evolution of gases (N_2, CO_2, Cl_2 and H_2O), yielding a solid with a sponge form. The resulting powders were calcined at 600°C for 2 hours (heating rate set at 5°C·min^{-1}), pelletized, crushed and sieved to 200–600 μm for catalytic tests. The temperature profile during the combustion reaction was recorded using a thermocouple connected to a data acquisition unit; the related temperature-time profiles are shown in Figure 1. All the combustion reactions were characterized by an abrupt rise in temperature from 100°C (water boiling point) to the maximum value. The measured flame temperature (Figure 1) increased from 991 to 1263°C by increasing the platinum load from 0.6 wt.% to 2.3 wt.%; this was due to the different amount of mixed precursors and fuel that determine an increase of the heat released by the reaction. For comparison, the CeO_2 support was synthesized by the same route; in this case the flame temperature reached 535°C (not shown). Losses associated with conduction/convection phenomena and possible delay of the thermocouple signal, during the sudden change of the temperature could affect the recorded values. The Pt content in the catalytic powders was confirmed by chemical analysis (ICP/OES), as reported in Table 1.

2.2. Catalyst Characterization

The specific surface area, estimated from adsorption/desorption isotherms at liquid nitrogen temperature (-196°C) on a *Micromeritics ASAP 2020* instrument, was calculated according to the Brunauer-Emmet-Teller (BET) equation.

X-ray diffraction (XRD) analysis were done with a *Philips X-Pert 3710* diffractometer using a Cu Kα radiation at 40 kV and 20 mA. Diffraction patterns were recorded in the scan ranges of 2θ = 20°-75° (1.50°·min^{-1}) and 2θ = 27°-30° (0.06°·min^{-1}). The peaks were assigned according to the PCPFWIN database. The crystallite size was calculated by the Scherrer equation from the most intense CeO_2 (111) reflecting planes, while the CeO_2 lattice parameter (α) was derived from the related patterns at low scan rate.

The platinum dispersion was measured by CO-pulse chemisorption method proposed by Takeguchi et al. [39], using a *Micromeritics ChemiSorb 2750* instruments equipped with a TCD detector. A mixture of 10% CO in He was injected in pulses of 600 NμL each, until the fulfilment of constant outlet peaks. Before measurements all the catalysts were: i) reduced under pure H_2 flow (30 Nml·min^{-1}) for 30 min at 200°C; ii) oxidized under pure O_2 flow (30 Nml·min^{-1}) for 10 min at room temperature; iii) treated under CO_2 flow (30 Nml·min^{-1}) for 10 min at room temperature; iv) reduced under pure H_2 flow (30 Nml·min^{-1}) for 30 min at room temperature; with this method the CO adsorption on CeO_2, as carbonate species is avoided.

On the same apparatus, the reducibility of the catalysts was studied by H_2 temperature-programmed reduction (H_2-TPR). A continuous flow of 5% H_2/Ar (30 Nml·min^{-1}) followed over the catalyst and the temperature was raised from -

80°C up to 1000°C with a rate of 20°C·min^{-1}. Before measurements all the catalyst samples were treated in situ under pure O_2 flow for 30 min at 200°C. The H_2 consumption was monitored by a thermal conductivity detector (TCD) and the response was quantitatively calibrated from the TPR area of known amounts of CuO. The reduction degree of PtO_x samples was calculated from the ratio between the H_2 consumption to the theoretical H_2 required to reduce all the metal oxide.

O_2 temperature-programmed oxidation (O_2-TPO) was performed by using the same apparatus; the sample was pre-treated with He (30 Nml·min^{-1}) raising the temperature up to 1000°C with a rate of 20°C·min^{-1}. The CO_2 production was monitored by a quadrupole mass spectrometer (*QMS Thermo Scientific ProLab*); the response was quantitatively calibrated from the TPO area of known amounts of $CaCO_3$.

The morphology of fresh, used and regenerated catalysts was studied by Transmission Electron Microscopy (TEM) using a *Philips CM12* instrument. Specimens were prepared by ultrasonic dispersion of the powders in isopropyl alcohol then deposited on a holey copper grid.

2.3. Steam Reforming Experiments

The flow sheet and the main components of the test-rig employed in the present study are shown in Figure 2. Two HPLC pumps (*Agilent 1260 Infinity Binary Pump*) were used to inject fuel (n-dodecane, from Sigma Aldrich) and steam into separated vaporizers/mixers. H_2O was injected/gasified in the first evaporator maintained at 340°C and then transferred, using N_2 as carrier, to the second evaporator heated at 300°C in which n-dodecane was injected/gasified. High purity N_2 (99.999%, from Rivoira) was used in the experiments, keeping constant flow rate by using mass flow controllers (*Brooks Instrument Smart Mass Flow*). The mass balance (C, O and H) of the reactant mixture fed to the reactor (heated at 340°C) was used to determine the related evaporation degree; the complete vaporization, with mass balance values of ca. 99-101%, was derived. Similarly, a mass balance of 100±2% during all the catalytic experiments was obtained. The gaseous mixture was sent to the fixed-bed reactor (i.d.=0.6 cm), inserted into a furnace heated with a PID temperature controller. The pelletized catalyst (0.6g; 200–600 μm) diluted with 0.6 g of quartz particles (200–600 μm) was used in order to ensure an optimal temperature distribution through the catalytic bed. The catalysts were pre-reduced in situ with 50% H_2/N_2 stream at 200°C for 1 hour; then, the reactor was purged in N_2 flow and heated to the reaction temperature. The catalytic performances were measured at atmospheric pressure by 6 hours tests; at the end of the experiments the reactor was switched off and cooled down to room temperature under N_2 flow. Stability tests were performed over 50 hours of time-on-stream by sequential start-up and shut-down cycles of ca. 6 hours each. The reaction temperature was measured and controlled by three K-type chromel-alumel thermocouples. One thermocouple was positioned inside the catalytic bed to regulate the set temperature (T_{SET} = 800°C) with a temperature programmable

controller (*Omron, E5AK-TAA2005*), while the others two were kept at the inlet (T_{IN}) and at the outlet (T_{OUT}) of the catalytic bed. The effects of steam-to-carbon molar ratio (S/C = 2-3), space velocity (GHSV = 16,000-32,000 h^{-1}, as gas hourly space velocity of gases fed at 0°C and 1 bar per volume of catalyst) and platinum loading (Pt = 0.6-2.3 wt.%) on the activity of Pt/CeO_2 catalysts were evaluated. Additional tests were carried out at low steam-to-carbon molar ratio (S/C = 1.5) and high space velocity (GHSV = 40000 h^{-1}) under start-up and shut-down cycles, in order to observe the catalysts deactivation. After each cycle, the reactor was flushed with N_2 decreasing the temperature from 800°C to 25°C; then the regeneration process with air was done by re-increasing the temperature to 800°C. The CO_2 peak, revealed during this step, indicated the combustion of carbon deposits.

The product mixture was periodically analyzed (every 15 minutes) by an online Gas Chromatograph (*Agilent 5975C series 4C/MSD*) equipped with TCD and FID detectors and mass spectrometer. N_2 was used as internal standard for mass balance calibration. The catalytic activity was reported as n-dodecane conversion (X_{C12H26}), molar concentrations (on dry and N_2-free basis) of H_2, CO, CO_2, CH_4, by-products (C_2H_6, C_2H_4, C_3H_8, C_3H_6) and H_2/CO molar ratio. The experimental results were compared with the thermodynamic equilibrium values calculated by a commercial steady-state simulation package named *HSC Chemistry 7.1®*, based on the minimization of Gibbs free-energy of each of the existing species ($C_{12}H_{26}$, CH_4, H_2O, CO_2, CO, H_2, C-containing by-products and solid carbon). The calculation was carried out at the reaction temperature (T_{SET} = 800°C).

3. Results and Discussion

3.1. Catalysts Characterization

The main textural and structural characteristics of the synthesized Pt/CeO_2 catalysts, compared with the CeO_2 support, are reported in Table 1. Pt/CeO_2 samples exhibited specific surface areas varying in the range of 8-12 m^2/g, lower than 22 m^2/g obtained for the CeO_2; this could be due to the effect of flame temperature recorded during the combustion synthesis, higher with Pt/CeO_2 catalysts (991-1263°C) than with CeO_2 (535°C) [37,38]. XRD patterns of calcined CeO_2 sample and Pt/CeO_2 catalysts are shown in Figure 3, while the related CeO_2 crystallite sizes and lattice parameters are included in Table 1. All the systems were characterized by a typical cubic fluorite structure of ceria, corresponding to the (111), (200), (220), (311), (222), and (400) reflection planes. No clear evidence of Pt active phase could be noticed; this could be ascribed to the presence of small and well distributed particles or small amount not reveleable by diffraction. The average crystallite size of the samples, calculated by the Scherrer equation (Table 1), indicated particles size of 11.4 nm for the CeO_2 sample, that slightly increased to 23.7-27.1 nm for Pt/CeO_2 systems; this evidence could be related to the preparation methodology. As previously reported, morphological characteristics of combustion-synthesized powders are closely related to the nature of combustion, mainly combustion enthalpy and flame

temperature [37,38]. It is evident that lower flame temperatures (Figure 1) led to lower CeO_2 crystallite size (Table 1). Besides, as shown in Figure 3, ceria reflections of Pt/CeO_2 systems were slight shifted to higher degrees in comparison to those of pure CeO_2, in accordance with the lattice contraction reported in Table 1. Pt/CeO_2 lattice contraction (5.386-5.389 Å compared to 5.394 of CeO_2) indicated the partial incorporation of smaller Pt ions (Pt^{4+} ionic radius = 0.62 Å or Pt^{2+} ionic radius = 0.80 Å) into the lattice of ceria Ce^{4+} (Ce^{4+} ionic radius = 0.97 Å) to form a solid solution [40].

TEM micrographs of the studied catalysts are displayed in Figure 4, while the derived Pt particle sizes are reported in Table 1. As can be seen, all the catalysts appeared well dispersed with a narrow particle size distribution. Particularly, the 0.6-Pt/CeO_2 sample (Figure 4a) showed Pt particles ranging between 2-4 nm. At increasing Pt loading, the Pt particle size increased to 5-7 nm and 7-9 nm for 1.2-Pt/CeO_2 (Figure 4b) and 2.3-Pt/CeO_2 (Figure 4c) samples, respectively. Pt particle growth could depend on two different factors, namely higher Pt loading on the ceria surface and greater heat released during the solution combustion synthesis. Indeed, flame temperature (Figure 1) increased from 991°C to 1263°C with increasing platinum load, resulting in Pt particles growth due to the sintering phenomena. These evidences were in good agreement with the CO-chemisorption results reported in Table 1. The trend of Pt particle size in relation to the Pt loading is the same. As a consequence, 0.6-Pt/CeO_2 sample showed higher dispersion value (26.7%) than 1.2-Pt/CeO_2 (8.7%) and 2.3-Pt/CeO_2 (3.9%) catalysts.

Figure 5 compares the H_2-TPR profiles of CeO_2 and Pt/CeO_2 catalysts. The quantitative estimation of the reduction peaks, related only to the platinum species, is reported in Table 2. For bare ceria, two main reduction peaks were observed, at approximately 500 and 930°C, respectively. As reported in literature, the low-temperature peak is due to the reduction of CeO_2 surface oxygen, while the high-temperature peak is due to the reduction of CeO_2 bulk oxygen [36,41]. The presence of platinum induced significant modifications in the reduction profile, especially in the low temperature zone; the TPR patterns are divided into three temperature regions: region I (-80–20°C), region II (20–350°C) and region III (350–1020°C).

Region I could be associated to removal of the readily available surface oxygen adjacent to the metal, through a spillover mechanism; all catalysts presented a single and symmetric peak at sub-ambient temperature, that could be assigned to the reduction of well dispersed platinum oxide species with uniform particle size distribution [40,42]. The sub-ambient peak was shifted to higher temperature (Table 2) with increasing Pt loading. Moreover, hydrogen consumption could be correlated to the size of Pt oxide particles. Indeed, H_2 consumption increased from 0.6 to 1.1 $mmol_{H2}/g_{PtO2}$ with decreasing Pt loading from 2.25 to 1.13 wt.%, due to the presence of smaller PtO_x particles. However, further reduction of Pt content (0.57 wt.%) led to a decrease in hydrogen consumption (0.04 $mmol_{H2}/g_{PtO2}$). In this case, very small PtO_x particles were more affected by support and, consequently, could be reduced at higher temperature [42,43].

Region II could be correlated to the reduction of PtO_x interacting with the support and to the formation of Pt-Ce solid solution. Moreover, the contribution of CeO_2 surface reduction caused by H_2 spillover effect (especially 0.6 wt.% Pt/CeO_2 catalyst) cannot be excluded [40,44]. Indeed, hydrogen, after dissociation on metallic Pt, was able to spillover to CeO_2 and to reduce it at lower temperatures [45,46]. Hydrogen consumption decreased from 13.4 to 1.6 $mmol_{H2}/g_{PtO2}$ by increasing Pt loading from 0.57 to 2.25 wt.%. This could be due to different concomitant reasons, as well as the increase in platinum particle size and the decrease in Pt-Ce solid solution formation, as confirmed by XRD studies (Figure 3, Table 1). Moreover, 0.6 wt.% Pt/CeO_2 reduction profile in region II showed evident differences compared to the other samples. The broad peak in the range 30-300°C also contained the contribution of the reduction of Ce^{4+} ions adjacent to Pt species due to a spillover effect, because the amount of hydrogen consumption (13.4 $mmol_{H2}/g_{PtO2}$) was significantly higher than the nominal values [42,45,46].

Region III could be ascribed to CeO_2 bulk oxygen reduction, which was only slightly affected by Pt presence [47] and for this reason it is not quantified.

3.2. Non-Catalytic Experiments (Blank Tests)

One of the main problems that affect the catalyst performances during reforming of liquid hydrocarbon fuels is the deactivation by carbon/coke formation. The thermal cracking of long chain hydrocarbons as n-dodecane may result in the formation of a mixture of lower hydrocarbons that, in turn, could cause carbon or coke deposition [10,14,15]. Preliminary blank tests were carried out in order to determine the temperature range inside where n-dodecane cracking reaction could occur. Figure 6a shows the scheme of the model reactor (quartz tube and furnace) for in-situ measurements of the temperature profile along the quartz tube. The temperature (T_C) was controlled by one K-type chromel-alumel thermocouple centered within the quartz reactor, while other six thermocouples were positioned along the reactor to measure the temperatures (T1, T2, T3, T4, T5, T6) between the inlet and the outlet (Figure 6a). Blank tests were carried out varying temperature (T_C = 400-700°C) at S/C = 2, with a total mixture ($C_{12}H_{26}$, N_2, H_2O) flow equal to 100 $Nml \cdot min^{-1}$, without catalyst. Temperature profiles for each test were registered and associated with the formation of visible carbon inside the reactor and with the ethylene formation revealed by the GC/MS analysis of the outlet products. Tests results, reported in Figure 6b, indicated that carbon deposition and ethylene formation were observed at temperatures higher than 550°C. Thus, n-dodecane cracking could occur at temperatures higher than 550°C.

Based on the obtained results, a bed configuration with an optimized temperature-control (Figure 6c) was adopted for catalytic tests, in order to avoid/minimize carbon formation due to cracking phenomena, especially at the inlet of the catalytic bed. The position of the catalytic bed within the furnace was determined in order to have an opportune temperature gradient between the inlet and the outlet (Figure 6c). Figure 6d shows the temperature profile recorded

during a catalytic test carried out at T_{SET} = 800°C, S/C = 2, GHSV = 24,000 h^{-1} with 1.2-Pt/CeO_2 catalyst. With this configuration, the temperature of the catalytic bed increased from 490 (T_{IN}) to 800°C (T_{SET}). Thus, the inlet temperature (490°C) remained lower than the cracking ignition temperature (550°C), avoiding the thermal cracking in the front part of the catalytic bed. However, a partial decomposition of n-dodecane into short-chain hydrocarbons (C1 – C11) probably occurred in the first part of the bed at lower temperature; these hydrocarbons could then be converted in the second part of catalytic bed at higher temperatures.

3.3. Catalytic Activity

3.3.1. Influence of steam-to-carbon molar ratio on the activity of the 1.2-Pt/CeO_2 catalyst

Figure 7 shows the influence of steam-to-carbon molar ratio (S/C = 2-3) on the activity of the 1.2-Pt/CeO_2 catalyst towards n-dodecane SR at T_{SET} = 800°C and GHSV = 24,000 h^{-1}. Results are reported in terms of n-dodecane conversion (X_{C12H26}) and product concentrations (H_2, CO, CO_2, CH_4 and C_2H_4, on dry and N_2-free basis). Experimental results are compared to thermodynamic equilibrium values, calculated at 800°C. It can be seen that n-dodecane conversion was total at all the investigated S/C molar ratios. The results showed that the increase of S/C ratio did not have an evident effect on the catalyst performance. H_2 concentration slightly increased from 70.7 to 71.7%, while almost constant CO (14.8-15.1%) and CO_2 (12.8-13.4%) concentrations were recorded in all the investigated S/C range. Constant traces of CH_4 (ca. 0.4%) and C_2H_4 (ca. 0.2%) were also revealed. The presence of other hydrocarbons that fell below the detection limits (< 0.05%) could not be excluded.

It is clearly evident that CO and CO_2 concentrations differed from equilibrium values. In particular, products mixture contained lower amount of CO and higher amount of CO_2 compared to the thermodynamic composition at all the studied S/C molar ratio. Besides, H_2O conversion (69.9-49.7%) resulted higher than equilibrium values (62.6-46.9%). This was mainly due to the temperature gradient present along the catalytic bed and described on section 3.2, while the thermodynamic predicted values were derived at 800°C. Indeed, the temperature along the catalytic bed increased from 480 (T_{IN}) to 800°C (T_{SET}), suggesting that the contributions of WGS (Eq. 2) and methanation reactions ($CO+3H_2 \rightarrow CH_4+H_2O$, $\Delta H°_{298}$=-206.2 $kJ \cdot mol^{-1}$ and $CO_2+4H_2 \rightarrow CH_4+2H_2O$, $\Delta H°_{298}$=-165.0 $kJ \cdot mol^{-1}$) were more relevant than the predictable values (at 800°C) [48]. Whereby, the exothermic WGS and methanation reactions could be favored in the first part of the bed at lower temperature, inducing a low CO concentration and, consequently, a high H_2/CO (4.7-4.8) molar ratio, a high CO_2 concentration and a more high CH_4 content in the reformate.

Because steam prevents carbon/coke formation but, at the same time, requires more energy, S/C = 2.5 was selected for subsequent investigation, constituting a good compromise between catalytic and energetic efficiency of the related fuel processor.

3.3.2. Influence of space velocity on the activity of the1.2-Pt/CeO_2 catalyst

The effect of space velocity (GHSV = 16,000-32,000 h^{-1}) on the catalytic activity of 1.2-Pt/CeO_2 catalyst was investigated at T_{SET} = 800°C and S/C = 2.5. Results are shown in Figure 8, highlighting almost stable catalytic activity at all investigated GHSVs. However, the1.2-Pt/CeO_2 system showed higher performance at 16,000 h^{-1}, in terms of total fuel conversion (maintained also at 24,000 h^{-1}), higher hydrogen production (72.8%) and absence of by-products (CH_4, C_2H_6, C_2H_4), associated with a H_2/CO molar ratio of 4.8. Increasing the GHSV up to 32,000 h^{-1}, the catalytic activity slightly decreased as n-dodecane conversion (98.8%) and H_2 concentration (70.0%), while the amount of by-products slightly increased (CH_4=1.2%, C_2H_6=0.2%, C_2H_4=1.1%). Also in this case, the temperature gradient along the catalytic bed played a key role in determining final products concentration, with CO (14.7-15.2%) and CO_2 (12.0-13.0%) concentrations respectively lower and higher than equilibrium values (19.2% for CO and 10.0% for CO_2).

The slight loss of activity, recorded by increasing space velocity, could be due to different causes: n-dodecane steam reforming is a strongly endothermic reaction often limited by heat and mass transfer, especially in packed bed reactors [49,50]. These phenomena enhanced at higher space velocity, could contribute to the decrease of the catalytic performance. In addition, cold spots in the reactor cannot be excluded, due to high steam amount through the reactor [51]. Besides, the increase in the GHSV implied a short residence time of reagents on the surface active sites; this could be not sufficient to maintain the activity of the samples considering the low dispersion of Pt particles (8.7%, measured by chemisorption analysis). Whereby, GHSV ranging between 16,000 and 24,000 h^{-1} appeared to be a favourable option for n-dodecane steam reforming.

3.3.3. Influence of platinum loading on the activity of Pt/CeO_2 catalysts

Figure 9 shows the influence of platinum loading (0.6-2.3 wt.%) on the catalytic activity of the Pt/CeO_2 catalyst towards n-dodecane SR at T_{SET} = 800°C, S/C = 2.5 and GHSV = 24,000 h^{-1}. Although n-dodecane conversion was almost total for all the prepared catalysts, the H_2 concentration slightly decreased from 71.7 to 68.8% by increasing the platinum loading from 0.57 to 1.13 wt.%. Indeed, the increase of noble metal content did not positively affect the catalyst performance. Particularly, 0.57 wt % Pt/CeO_2 system showed total n-dodecane conversion and higher H_2 concentration (71.7%) in absence of by-products. Increasing noble metal loading up to 1.13 wt.%, n-dodecane conversion still remained complete, H_2 concentration slightly decreased to 71.4%, but low concentrations of CH_4 (0.4%) and C_2H_4 (0.3%) were detected. A further increase in Pt loading (2.25 wt.%) led to a decrease of the catalytic performance: the H_2 concentration decreased to 68.8% and the content of by-products increased (CH_4=2.1%,

C_2H_6=0.2%, C_2H_4=2.8%); in addition, the presence of other hydrocarbons (> C2) below the detection limit (< 0.05%) could not be excluded.

The low activity of the sample with high metal loading was probably related to physico-chemical and morphological properties of the catalysts. As reported in Table 1, the increase in platinum loading led to the decrease of metal dispersion (from CO-chemisorption) and the increase of Pt particle size (from TEM). As previously mentioned this behaviour could be related to the adopted solution combustion method and, particularly, to the heat released during the synthesis. The presence of larger Pt metal grains for 1.13 wt.% Pt/CeO_2 and especially for 2.25 wt.% Pt/CeO_2 systems led to the decrease of the catalytic performances. Moreover, higher Pt loadings could lead to the formation of multiple adjacent active sites promoting, in turn, additional coking, responsible for catalyst deactivation.

Conversely, the 0.6 wt.% Pt/CeO_2 system showed higher catalytic activity due to the presence of small and homogeneously distributed Pt particles on the ceria support.

3.4. Stability Tests

3.4.1. Time-on-stream experiments

Figure 10a shows the performance of 0.6-Pt/CeO_2 catalyst towards n-dodecane SR T_{SET} = 800°C, S/C = 2.5 and GHSV = 16,000 h^{-1} during 50 hours of time-on-stream. Stability tests were carried out with successive start-up and shut-down cycles of ca. 6 hours each. Moreover, catalytic performance of commercial Rh/ZDC (Rh/Zirconia-doped-Ceria) catalyst was also reported in Figure 10b as comparison. The aim of this test was to investigate carbon/coke formation phenomena, highlighting the applicability of the optimized temperature-controlled bed configuration (Figure 6), designed and implemented to overcome one of the major problems related to reforming of liquid hydrocarbons reforming [10]. The 0.6-Pt/CeO_2 catalyst showed good and stable performances in terms of total n-dodecane conversion (not reported) and H_2 concentration (ca. 73%). No relevant deactivation of the catalyst was observed throughout 50 hours of reaction, but low production of CH_4 (ca. 0.2%) and C_2H_4 (ca. 0.1%) was envisaged after 24 and 34 hours of test, respectively. In addition, the Pt-based system (Figure 10a) showed catalytic activity and stability similar to that of commercial Rh-based system (Figure 10b). The low amount and cost of the Pt sample (0.6 wt.% of Pt), related to the commercially available Rh-based catalyst (2.0 wt.% of Rh), can make it as a promising catalyst for diesel reforming.

The regeneration ability of the catalyst was evaluated during further tests carried out at lower steam-to-carbon molar ratio (S/C = 1.5) and higher space velocity (GHSV = 40,000 h^{-1}) under sequential start-up and shut-down cycles. In this conditions, as evidenced in Figure 11, the performance of the catalyst decreased: the H_2 and CO concentration in the reformate gases decreased during the first 5h of test; while a progressive increase in the CO_2 and by-products

concentration could be observed. After the regeneration step with air, the initial gas concentration in the reformate was restored, indicating that the full regeneration of the catalyst is possible.

Promising activity of the 0.6 wt.% Pt/CeO_2 catalyst could be associated to different contributions. The adopted catalytic bed configuration allowed avoiding/minimizing carbon/coke formation, especially at the inlet of the catalytic bed. Besides, the use of ceria as support played another significant role in SR of n-dodecane. The principal role of ceria was connected with the ability to increase the adsorption of steam by its vacant oxygen and to transfer oxygen to the supported metallic site, keeping the surface relatively free of carbon. This self-decoking capability of ceria-based catalysts, due to the gasification reaction by oxygen species from the lattice, was previously studied and discussed by other authors [52-55] and also in our previous papers [34,36,40,56,57]. In addition, partial incorporation of Pt ions into the ceria matrix to form Pt-Ce solid solution (as revealed from XRD and TPR analysis) enhanced oxygen mobility by increasing CeO_2 structural defects. This further limited carbon deposition on the catalyst surface. Moreover, small particles were determined for 0.6 wt.% Pt/CeO_2 catalyst (TEM analysis). As reported in literature, coke and carbon (graphite or filamentous) carbon involves the formation of C–C bonds on multiple atoms sites, resulting structure-sensitive, i.e. sensitive to surface structure and metal crystallite size [58,59]. Bitter et al. [60] found that catalysts containing larger Pt crystallites deactivated more rapidly than those containing small crystallites. The 0.6-Pt/CeO_2 catalyst constituted a promising catalytic system for n-dodecane SR reaction.

3.4.2. Characterization of 0.6-Pt/CeO_2 used-regenerated catalyst

Figure 12 shows the TPO profile of the used 0.6-Pt/CeO_2 catalyst after the stability test. The analysis evidenced a carbon formation rate equal to 0.2 $mg_{carbon} \cdot g_{cat}^{-1} \cdot h^{-1}$ (corresponding to ca. 0.7 wt.%), suggesting good carbon resistance after 50 hours of time-on-stream. Several CO_2 peaks were observed, indicating different types of carbonaceous species with different reactivity toward oxidation. Contrarily, no peaks were found in the TPO profile of the commercial catalyst (not shown). As reported in Rostrup-Nielsen's review [7], three types of carbon were identified on steam reforming catalysts: i) pyrolitic (derived from thermal cracking of hydrocarbons at temperatures higher than 597°C and low S/C ratios); ii) filamentous (produced at temperatures above 447°C and low S/C ratios); iii) encapsulating (non reactive film with C-H bonds produced through polymerization at temperatures below 497°C and low S/C ratios). The formation of these carbon species was influenced by several parameters, such as catalyst (surface properties), feed composition (hydrocarbon, S/C ratio) and reaction temperature. As shown in Figure 11, low-temperature peaks (195 and 350°C) could be associated to the formation of soft or surface sensitive carbon deposits [61,62]. A widely accepted interpretation of these peaks is that they correspond to more reactive carbon or species located at metal/support interfaces [63,64]. The large CO_2 peak at ca. 605°C could be associated to pyrolitic carbon, formed by

cracking/decomposition of n-dodecane or low chain hydrocarbons [61,65]. Some authors suggested that this peak corresponds to less reactive carbon species deposited on the support [63-65].

Figure 13 shows the TEM images of the used and regenerated 0.6-Pt/CeO_2 catalysts. By comparing the TEM micrographs of fresh (Figure 4a) and used-regenerated samples, the morphological structure of the catalyst did not show any relevant changes. After stability test, Pt particles appeared small and well distributed with size ranging from 2.5 to 4.5 nm (Figure 13a). Moreover, only traces of carbon deposition were noticed. The absence of severe particles aggregation on spent catalysts denoted that metal sintering on the support surface was not a dominant phenomenon under the investigated conditions, which is in agreement with the good catalytic performances recorded during the 50 hours of time-on-stream. Moreover, TEM image of the regenerated system (Figure 13b) showed that the regeneration process carried out to remove carbon deposited during the reforming process, did not affect the size of platinum particles (2-5 nm), signal of a good resistance to metal sintering of the studied catalyst.

3.5. Conclusions

In this study, catalytic activity of Pt/CeO_2 catalysts (0.6-2.2 wt% of metal loading) was probed towards steam reforming of n-dodecane, as model compound of marine diesel. The effect of steam-to-carbon molar ratio (S/C = 2-3), space velocity (GHSV = 16,000-32,000 h^{-1}) and time-on-stream were also evaluated. Catalysts were prepared by solution combustion synthesis (SCS) and characterized by XRD, N_2-physisorption, CO-chemisorption, TPR, TPO and TEM techniques. Between the prepared catalysts, 0.6-Pt/CeO_2 sample showed high catalytic activity in terms of total n-dodecane conversion and high H_2 concentration (ca. 73%, dry and N_2-free basis) at T_{SET} = 800°C, S/C = 2.5 and GHSV = 16,000 h^{-1}. The Pt-based catalyst showed stable performance during 50 hours of reaction, with an activity similar to that of a commercial Rh-based system.

A special bed configuration with an adequate temperature control allowed limiting/avoiding carbon/coke formation due to n-dodecane cracking phenomena, especially at the inlet of the catalytic bed. Temperature gradient (ca. 480-800°C) along the catalytic bed played a key role in determining final products concentration due to the occurrence of WGS equilibrium reaction.

Physico-chemical and morphological properties of the 0.6-Pt/CeO_2 sample catalyst further limited carbon deposition on the catalyst surface, making it a promising active and stable system for n-dodecane steam reforming reaction.

Acknowledgements

This work was funded by the Italian Ministry of Education, University and Research, MIUR. “PON Ricerca e Competività”, in the framework of the “TESEO” (High Efficiency Technologies for Energy and Environmental Sustainability On-board) project.

References

[1]. R.C. Samsun, J. Pasel, R. Peters, D. Stolten, Int. J. Hydrogen Energy 40 (2015) 6405–6421.

[2]. A.V. González, L.J. Pettersson, Catal. Today 210 (2013) 19–25.

[3]. T. Aicher, B. Lenz, F. Gschnell, U. Groos, F. Federici, L. Caprile, L. Parodi, J. Power Sources 154 (2006) 503–508.

[4]. S.Y. Jung, D.G. Ju, E.J. Lim, S.C. Lee, B.W. Hwang, J.C. Kim, Int. J. Hydrogen Energy 40 (2015) 13412–13422.

[5]. G. Dolanc, B. Pregelj, J. Petrovčič, J. Pasel, G. Kolb, J. Power Sources 313 (2016) 223–232.

[6]. R.R. Kondakindi, A. Kundu, K. Karan, B.A. Peppley, A. Qi, C. Thurgood, P. Schurer, Appl. Catal. A 390 (2010) 271–280.

[7]. J.R. Rostrup–Nielsen, Catalytic steam reforming, in: J.R. Anderson, M. Boudart (Eds), Catal. Sci. Technol., vol. 5, Springer–Verlag, Berlin, 1984.

[8]. X. Xu, P. Li, Y. Shen, Appl. Energy 108 (2013) 202–217.

[9]. C.H. Bartholomew, Catal. Rev. Sci. Eng. 24 (1982) 67–112.

[10]. R.D. Parmar, A. Kundu, K. Karan, J. Power Sources 194 (2009) 1007–1020.

[11]. I.E. Achouri, N. Abatzoglou, C. Fauteux–Lefebvre, N. Braidy, Catal. Today 207 (2013) 13–20.

[12]. D. Shekhawat, D.A. Berry, T.H. Gardner, J.J. Spivey, in: J.J. Spivey, K.M. Dooley (Eds), Catalysis 19 (2006) 184–253.

[13]. I. Chen, D.–M. Shiue, Ind. Eng. Chem. Res. 27 (1988) 1391–1396.

[14]. X. Xu, P. Li, Y. Shen, Appl. Energy 108 (2013) 202–217.

[15]. Y. Chen, H. Xu, Y. Wang, X. Jin, G. Xiong, Fuel Process. Technol. 87 (2006) 971–978.

[16]. L. Hartmann, K. Lucka, H. Köhne, J. Power Sources 118 (2003) 286–297.

[17]. B. Lindström, J.A.J. Karlsson, P. Ekdunge, L. De Verlier, B. Häggendal, J. Dawody, M. Nilsson, L.J. Pettersson, Int. J. Hydrogen Energy 24 (2009) 3367–3381.

[18]. Z. Porš, J. Pasel, A. Tschauder, R. Dahl, R. Peters, D. Stolten, Fuel Cells 8 (2008) 129–137.

[19]. J. Pasel, J. Meibner, Z. Porš, R.C. Samsun, A. Tschauder, R. Peters, Int. J. Hydrogen Energy 32 (2007) 4847–4858.

[20]. S.M. An, Sang, W.S. Kim, S.Y. Lee, Int. J. Hydrogen Energy 36 (2011) 5342–5349.

[21]. K.Y. Koo, M.G. Park, U.H. Jung, S.H. Kim, Int. J. Hydrogen Energy 39 (2014) 10941–10950.

[22]. X. Xu, S. Zhang, P. Li, Int. J. Hydrogen Energy 39 (2014) 19593–19602.

[23]. A. Azad, M.J. Duran, Appl. Catal. A 330 (2007) 77–88.

[24]. A. Azad, M.J. Duran, A.K. McCoy, M.A. Abraham, Appl. Catal. A 332 (2007) 225–236.

[25]. J.T. Richardson, M. Garrait, J. Hung, Appl. Catal. A 255 (2003) 69–82.

[26]. M. Ferrandon, T. Krause, Appl. Catal. A 311 (2006) 135–145.

[27]. M. Ferrandon, A.J. Kropf, T. Krause, Appl. Catal. A 379 (2010) 121–128.

[28]. A.F. Ghenciu, Curr. Opin. Solid State Mater. Sci. 6 (2002) 389–399.

[29]. U. Hennings, R. Reimert, Appl. Catal. B 70 (2005) 498–508.

[30]. D. Shekhawat, T.H. Gardner, D.A. Berry, M. Salazar, D.J. Haynes, J.J. Spivey, Appl. Catal. A 311 (2006) 8–16.

[31]. C. Xie, Y. Chen, M.H. Engelhard, and C. Song, ACS Catal. 2 (2012) 1127–1137.

[32]. H.M. Li, Q.C. Zhu, Y.L. Li, M.C. Gong, Y.D. Chen, J.L. Wang, Y.Q. Chen, J. Rare Earths 28 (2010) 79–84.

[33]. A. Trovarelli, Catal. Rev.-Sci. Eng. 38(1996) 439–520.

[34]. L. Pino, A. Vita, F. Cipitì, M. Laganà, V. Recupero, Appl. Catal. A 306 (2006) 68–77.

[35]. C. Fabiano, C. Italiano, A. Vita, L. Pino, M. Laganà, V. Recupero, HYdrogen POwer Theoretical and Engineering Solutions International Symposium 2015, Toledo, Spain

[36]. L. Pino, A. Vita, F. Cipitì, M. Laganà, V. Recupero, Appl. Catal. B 104 (2011) 64–73.

[37]. C. Italiano, A. Vita, C. Fabiano, M. Laganà, L. Pino, Int. J. Hydrogen Energy 40 (2015) 11823–11830.

[38]. A. Vita, C. Italiano, C. Fabiano, M. Laganà, L. Pino, Mater. Chem. Phys. 163 (2015) 337–347.

[39]. T. Takeguchi, S. Manabe, R. Kikuchi, K. Eguchi, T. Kanazawa, S. Matsumoto, W. Ueda, Appl. Catal. A 293 (2005) 91–96.

[40]. L. Pino, A.Vita, M. Cordaro, V. Recupero, M. S. Hegde, Appl. Catal. A 243 (2003) 135–146.

[41]. J. Xiaoyuan, L. Guanglie, Z. Renxian, M. Jianxin, C. Yu, Z. Xiaoming, Appl. Surf. Sci. 173 (2001) 208–220.

[42]. H.-H. Liu, Y. Wang, A.-P. Jia, S.-Y. Wang, M.-F. Luo, J.-Q. Lu, Appl. Surf. Sci. 314 (2014) 725–734.

[43]. S.K. Meher, M. Cargnello, H. Troiani, T. Montini, G.R. Rao, P. Fornasiero, Appl. Catal. B 130 (2013) 121–131.

[44]. Z. He, X. Wang, Y. Pu, Z. Qian, Int. J. Hydrogen Energy 37 (2012) 11132–11140.

[45]. Y. Ji, A.M.J. van der Eerden, V. Koot, P. J. Kooyman, J.D. Meeldijk, B.M. Weckhuysen, D.K.C. Koningsberger, J. Catal. 234 (2005) 376–384.

[46]. T. Hou, B. Yu, S. Zhang, T. Xu, D. Wang, W. Cai, Catal. Commun. 58 (2015) 137–140.

[47]. S. Damyanova, B. Pawelec, K. Arishtirova, M.V. Martinez Huerta, J.L.G. Fierro, J.L.G. Fierro, Appl. Catal. B 89 (2009) 149–159.

[48]. R.A. Dagle, A. Karim, G. Li, Y. Su, D.L. King, Syngas conditioning, in: D. Shekhawat, J.J. Spivey and D.A. Berry (Eds.), Fuel cells: Technologies for fuel processing, Elsevier, 2011, pp. 361–408.

[49]. A. Vita, G. Cristiano, C. Italiano, L. Pino, S. Specchia, Appl. Catal. B 162 (2015) 551–563.

[50]. J.M. Bae S. Ahmed, R. Kumar, E. Doss, J. Power Sources 139 (2005) 91–95.

[51]. S. Martin, A. Wörner, J. Power Sources 196 (2011) 3163–3171.

[52]. M.D. Salazar-Villalpando, D.A. Berry, T.H. Gardner, Int. J. Hydrogen Energy 33 (2008) 2695–2703.

[53]. M. Salazar, D.A. Berry, T.H. Gardner, D. Shekhawat, D. Floyd, Appl. Catal. A 310 (2006) 54–60.

[54]. K. Tomishige, T. Kimura, J. Nishikawa, T. Miyazawa, K. Kunimori, Catal. Commun. 8 (2007) 1074–1079.

[55]. G. Nahar, V. Dupont, Renew. Sust. Energ. Review 32 (2014) 777–796.

[56]. L. Pino, A. Vita, F. Cipitì, M. Laganà, V. Recupero, Catal. Lett. 122 (2008) 121–130.

[57]. A. Vita, L. Pino, F. Cipitì, M. Laganà, V. Recupero, Fuel Process. Technol. 127 (2014) 47–58.

[58]. M.L. Toebles, J.H. Bitter, A.J. Van Dillen, K.P. de Jong, Catal. Today 76 (2002) 33–42.

[59]. K. Tao, S. Lei, Q. Ma, D. Wang, C. Zeng, C. Kong, M. Wu, L. Chen, S. Zhou, Y. Hu, N. Tsubaki, Chem. Eng. J. 221 (2013) 25–31.

[60]. J.H. Bitter, K. Seshan, J.A. Lercher, J. Catal. 183 (1999) 336–343.

[61]. B. D. Gould, X. Chen, J. W. Schwank, Appl. Catal. A 334 (2008) 277–290.

[62]. T.A. Westrich, X. Chen, J.W. Appl. Catal. A 386 (2010) 83–93.

[63]. A. Tanksale, J.N. Beltramini, J.A. Dumesic, G.Q. Lu, J. Catal. 258 (2008) 366–377.

[64]. A. Shamsi, J.P. Baltrus, J.J. Spivey, Appl. Catal. A 293 (2005) 145–152.

[65]. V.S. Gugilla, J. Akyurtlu, A. Akyurtlu, I. Blankson, Ind. Eng. Chem. Res. 49 (2010) 8164–8173.

Table Captions

Table 1. Main textural and structural properties of synthesized CeO_2 carrier and Pt/CeO_2 catalysts.

Table 2. Reducibility and reduction species for Pt/CeO_2 catalysts as a function of platinum loading.

Figure Captions

Figure 1. Experimental flame-temperature versus time plots during combustion reaction synthesis.

Figure 2. Global schematic diagram of the experimental setup.

Figure 3. XRD patterns of CeO_2 carrier and Pt/CeO_2 catalysts compared with the reference compound (CeO_2, JPDS 4-593).

Figure 4. TEM images of Pt/CeO_2 catalysts as a function of platinum loading: (a) 0.6-Pt/CeO_2; (b) 1.2-Pt/CeO_2; (c) 2.3-Pt/CeO_2.

Figure 5. H_2-TPR patterns of CeO_2 and Pt/CeO_2 samples.

Figure 6. (a) Scheme of model reactor (quartz tube and furnace) for blank tests; (b) Temperature profiles and carbon formation zone during blank tests (T_C = 400-700°C, S/C = 2); (c) Catalytic bed configuration for n-dodecane SR experiments; (d) temperature gradient profile during n-dodecane SR over 1.2-Pt/CeO_2 catalyst at T_{SET} = 800°C, S/C = 2 and GHSV=24,000 h^{-1}.

Figure 7. Influence of S/C molar ratio on n-dodecane SR over 1.2-Pt/CeO_2 catalyst: n-dodecane conversion, H_2, CO, CO_2 and by-products (CH_4, C_2H_4) concentrations (dry and N_2-free basis) and H_2/CO molar ratio. Equilibrium values are reported as dotted lines. Reaction conditions: T_{SET} = 800°C, S/C = 2.0-3.0, GHSV = 24,000 h^{-1}.

Figure 8. Influence of GHSV on n-dodecane SR over 1.2-Pt/CeO_2 catalyst: n-dodecane conversion, H_2, CO, CO_2 and by-products (CH_4, C_2H_6, C_2H_4) concentrations (dry and N_2-free basis) and H_2/CO molar ratio. Equilibrium values are reported as dotted lines. Reaction conditions: T_{SET} = 800°C, S/C = 2.5, GHSV = 16,000-32,000 h^{-1}.

Figure 9. Influence of platinum loading on n-dodecane SR over Pt/CeO_2 catalysts: n-dodecane conversion, H_2, CO, CO_2 and by-products (CH_4, C_2H_6, C_2H_4) concentrations (dry and N_2-free basis) and H_2/CO molar ratio. Equilibrium values are reported as dotted lines. Reaction conditions: T_{SET} = 800°C, S/C = 2.5, GHSV = 24,000 h^{-1}.

Figure 10. Stability test of n-dodecane SR over (a) 0.6-Pt/CeO_2 catalyst and (b) commercial Rh/ZDC (Rh/Zirconia-Doped-Ceria) catalyst: Product composition (dry and N_2-free basis) and H_2/CO molar ratio. Reaction conditions: T_{SET} = 800°C, S/C = 2.5, GHSV = 16,000 h^{-1}.

Figure 11. Regeneration test of 0.6-Pt/CeO_2 catalyst towards n-dodecane SR: Product composition (dry and N_2-free basis). Reaction conditions: T_{SET} = 800°C, S/C = 1.5, GHSV = 40,000 h^{-1}.

Figure 12. TPO pattern of used (stability test) 0.6- Pt/CeO_2 catalyst.

Figure 13. TEM micrograph of (a) used (stability test) and (b) regenerated 0.6-Pt/CeO_2 catalysts.

Table 1

Sample	Pt loading[a] (wt.%)	SA_{BET} (m^2/g)	X-ray		CO-Chemisorption		TEM
			CeO_2 crystallite size[b] (nm)	CeO_2 lattice parameter[b] (Å)	Pt particle size (nm)	Pt dispersion (%)	Pt particle size (nm)
CeO_2	-	21.8	11.4	5.394	-	-	-
0.6-Pt/CeO_2	0.57	12.1	23.7	5.386	4.2	26.7	2-4
1.2-Pt/CeO_2	1.13	9.1	27.0	5.387	13.1	8.7	5-7
2.3-Pt/CeO_2	2.25	8.4	27.1	5.389	28.7	3.9	7-9

[a] *Determined by chemical ICP/OES analysis;*

[b] *Calculated from X-ray diffraction: CeO_2 crystallite size from the Scherrer equation of the CeO_2 (111) reflection; Lattice parameter (α) from the relation* $\alpha = \sqrt{h^2 \cdot k^2 \cdot l^2} \cdot (\lambda / 2 \cdot \sin\theta)$

Table 2

		Platinum Reduction Zone			
		-80<T<20°C		20<T<350°C	
Sample	Reducibility (%)	H_2 consumption ($mmol_{H2}/g_{PtO2}$)	Maximun temperature (°C)	H_2 consumption ($mmol_{H2}/g_{PtO2}$)	Maximun temperature (°C)
0.6-Pt/CeO_2	>100	0.04	-49	13.36	100-165
1.2-Pt/CeO_2	32.8	1.06	-26	1.82	110
2.3-PtCeO_2	25.2	0.62	-14	1.60	128

Figure 1

Click here to download high resolution image

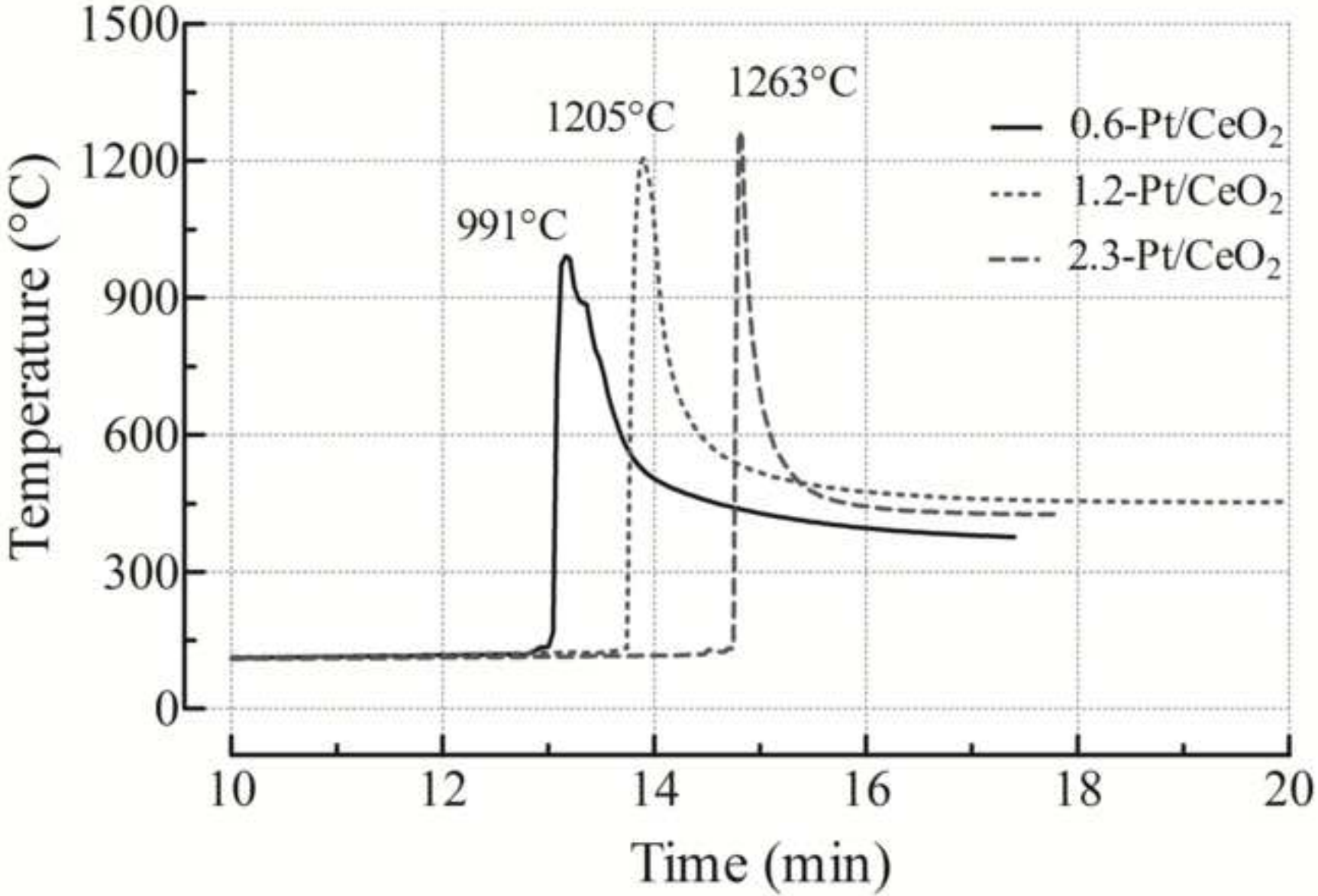

Figure 2

Click here to download high resolution image

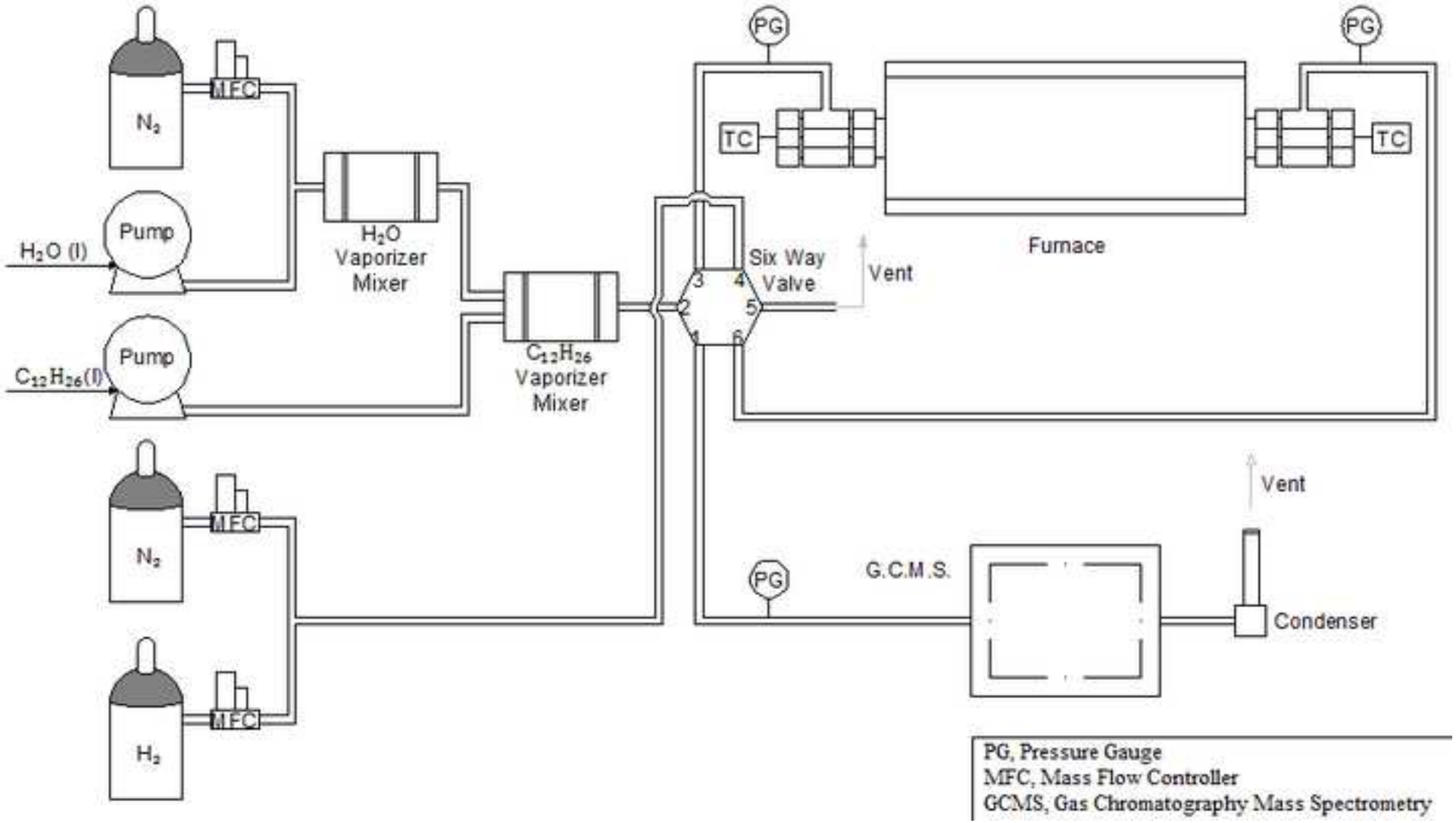

Figure 3

Click here to download high resolution image

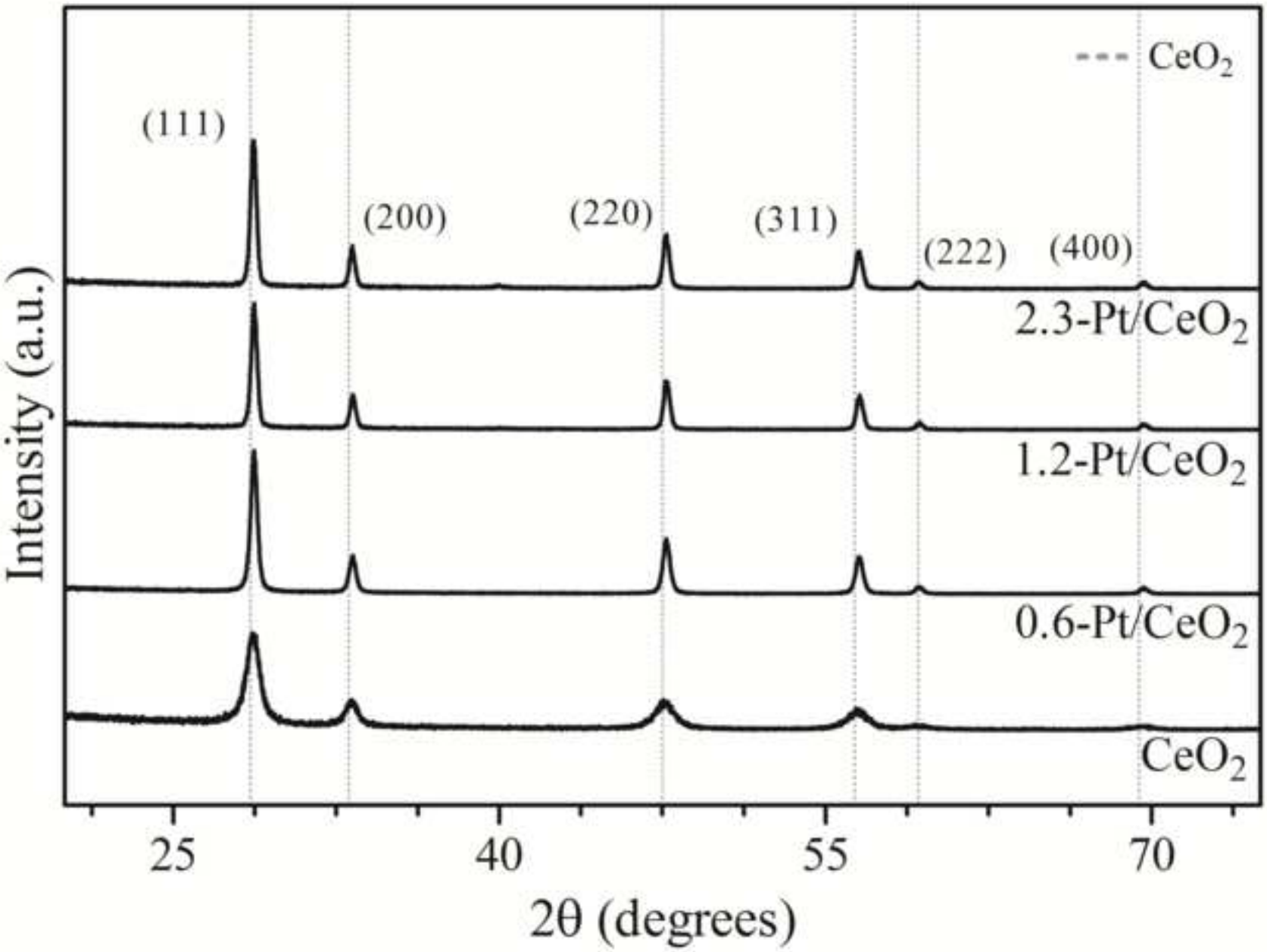

Figure 4

Click here to download high resolution image

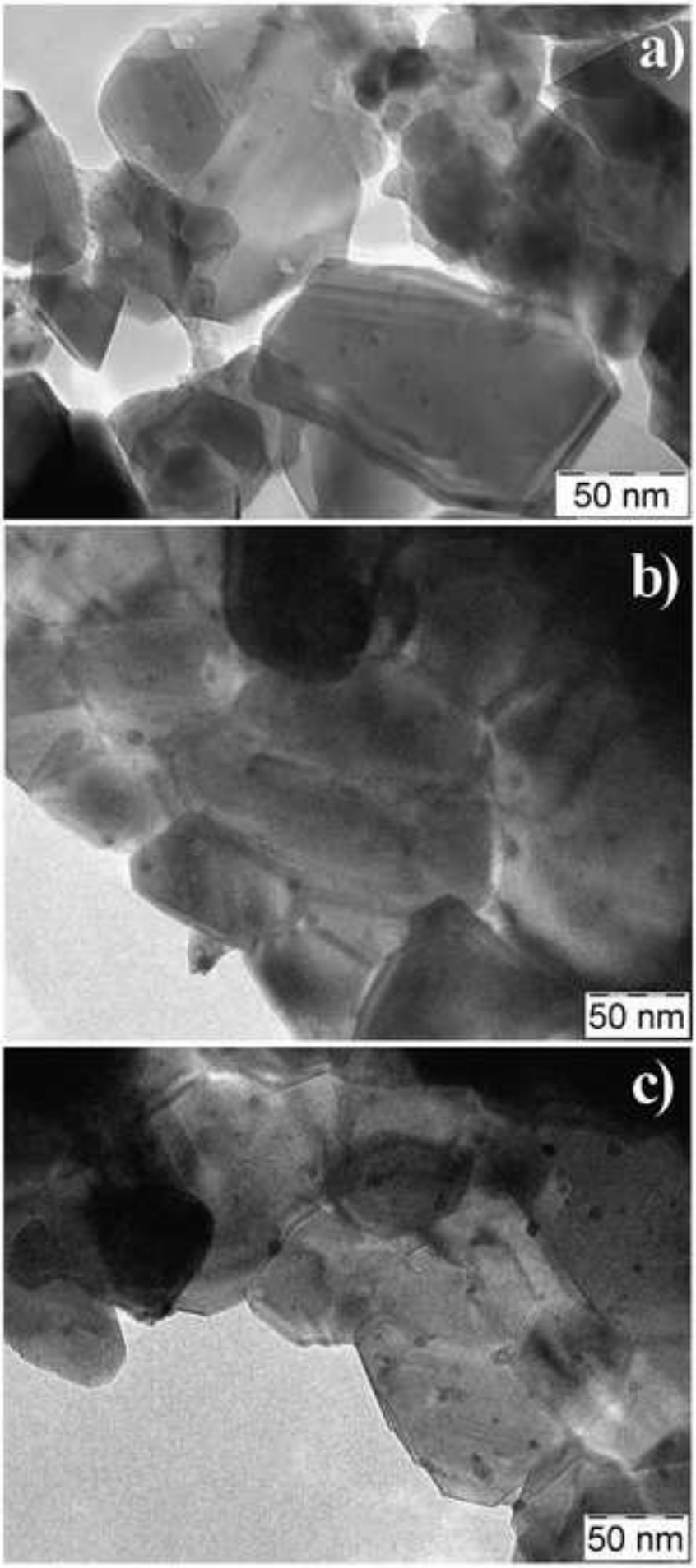

Figure 5

Click here to download high resolution image

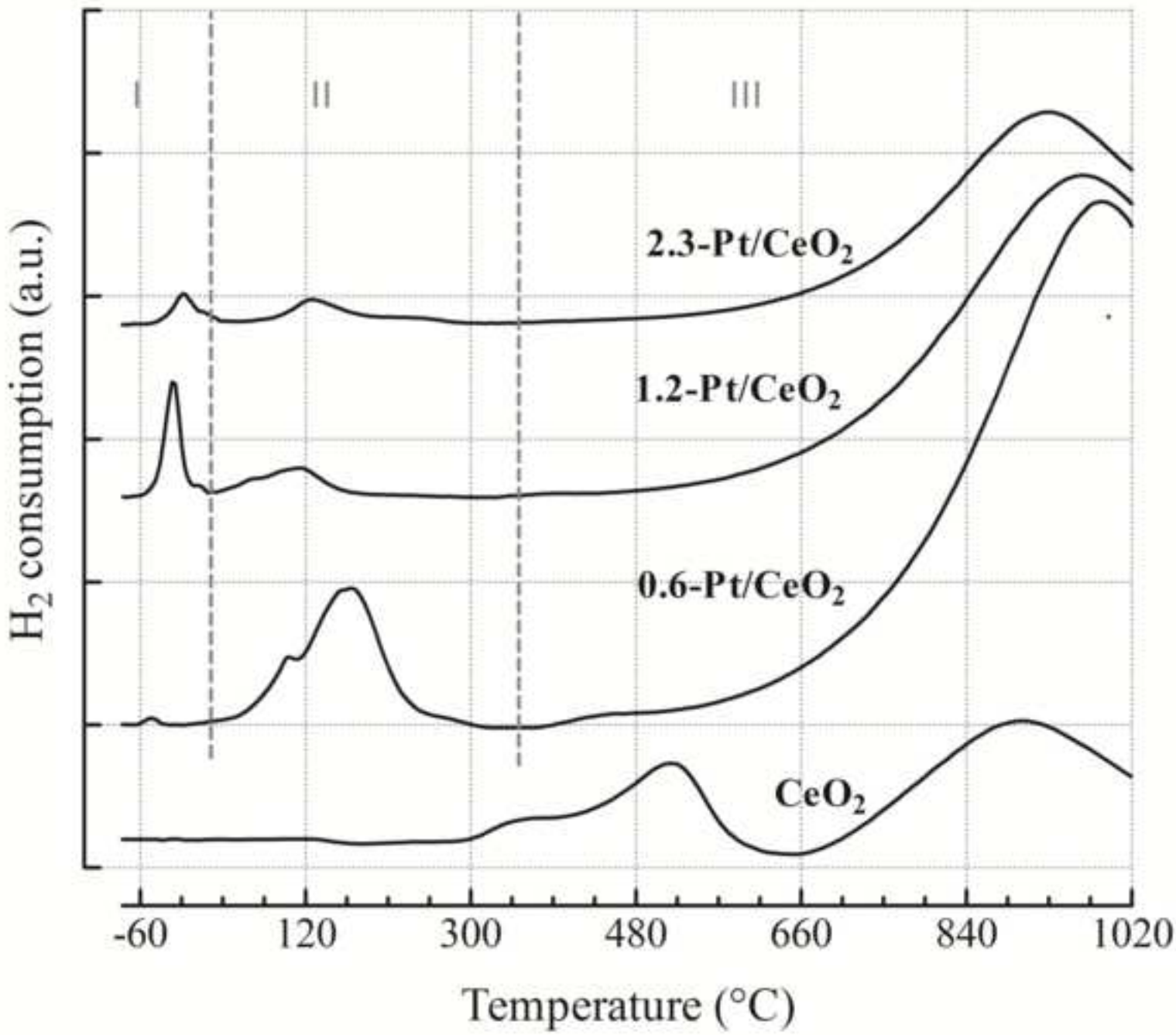

Figure 6

Click here to download high resolution image

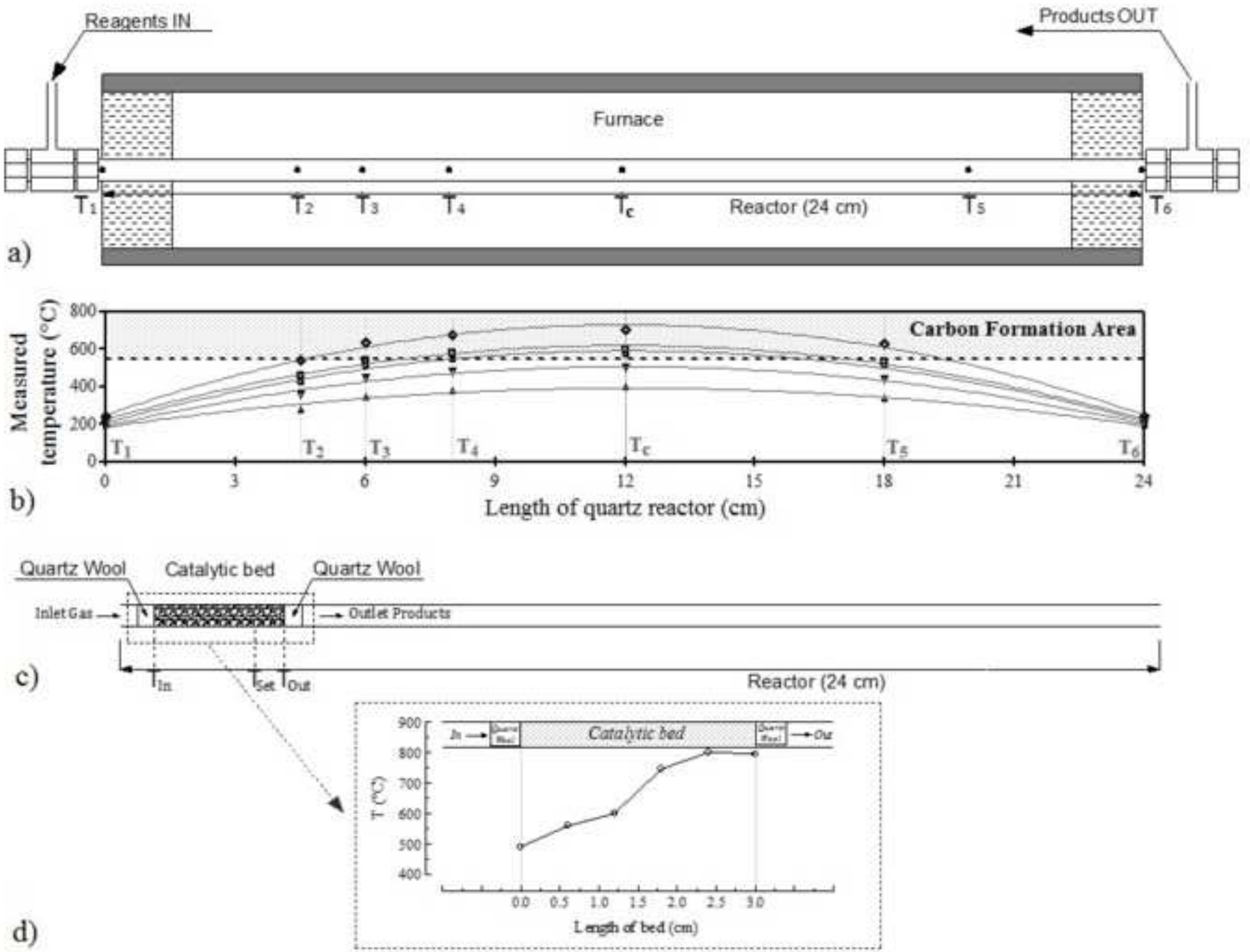

Figure 7

Click here to download high resolution image

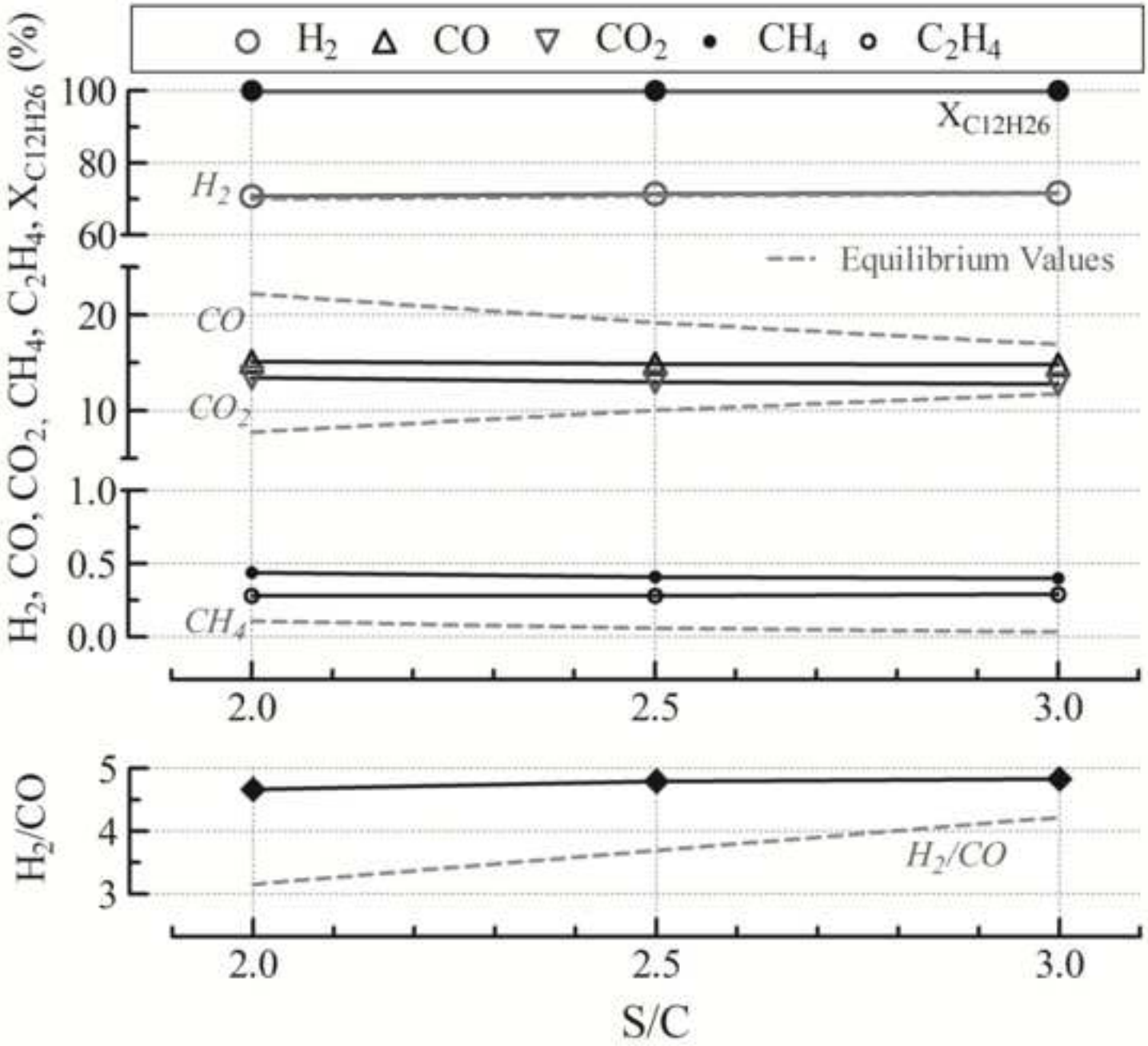

Figure 8

Click here to download high resolution image

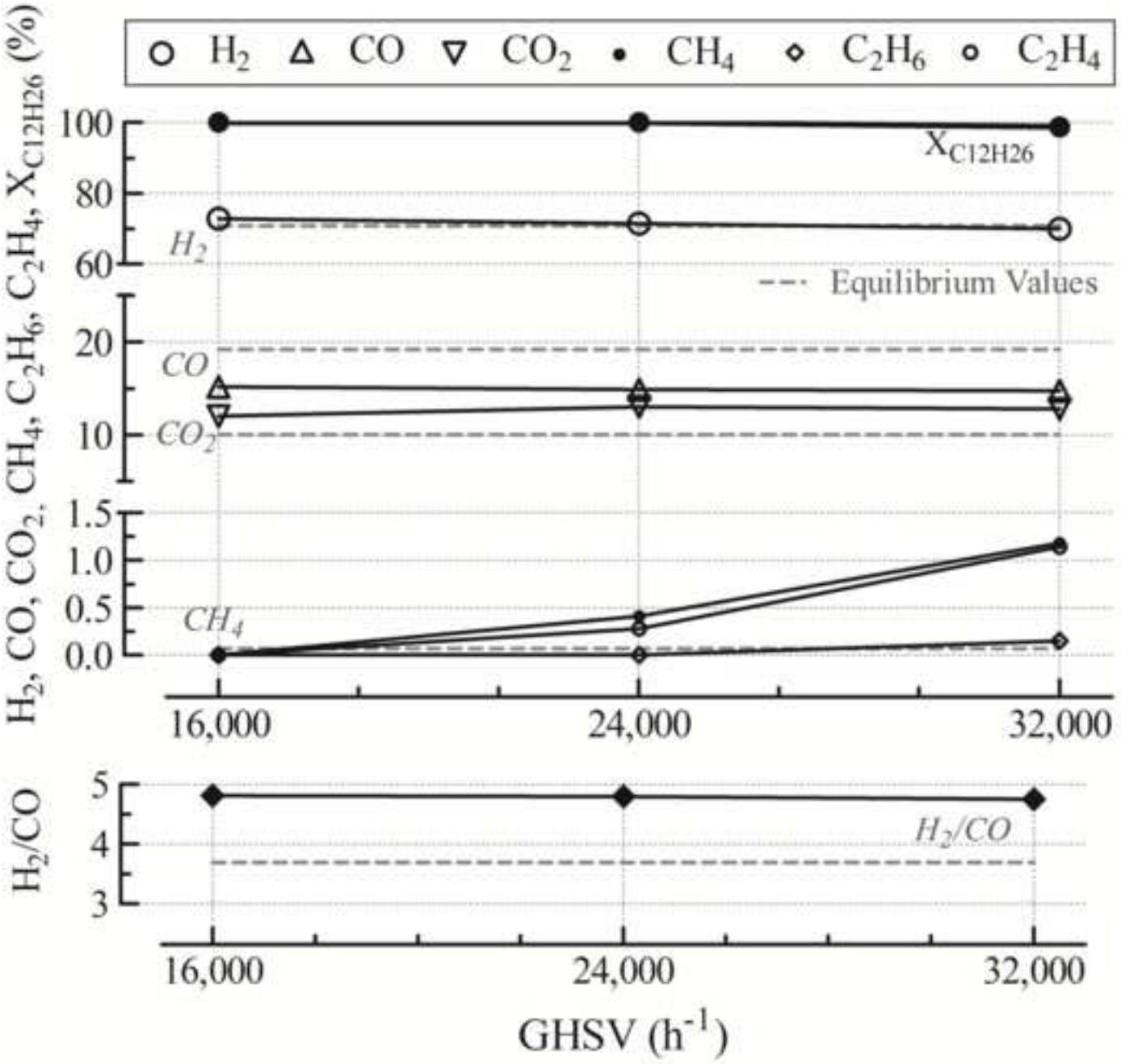

Figure 9

Click here to download high resolution image

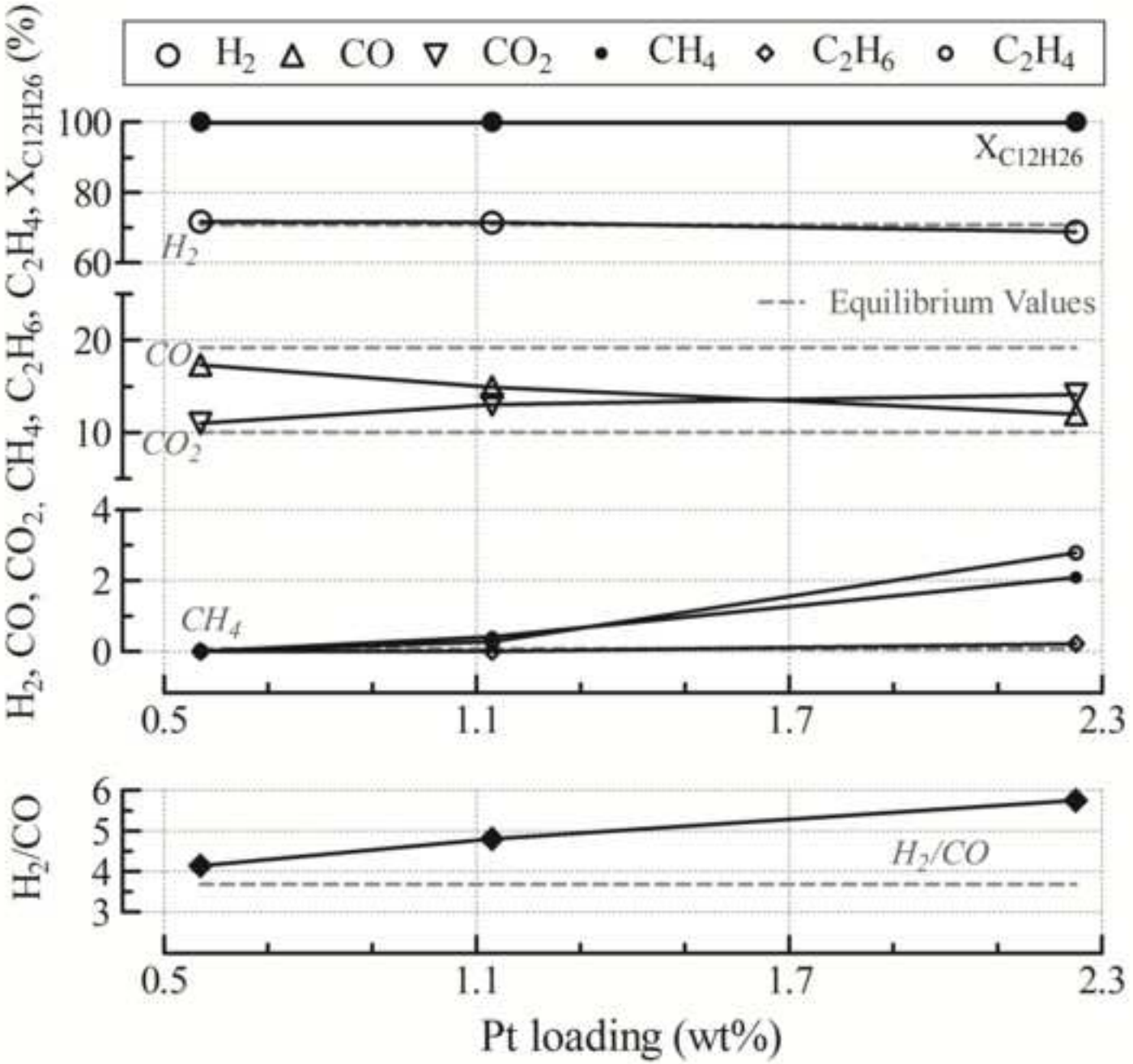

Figure 10 rev

Click here to download high resolution image

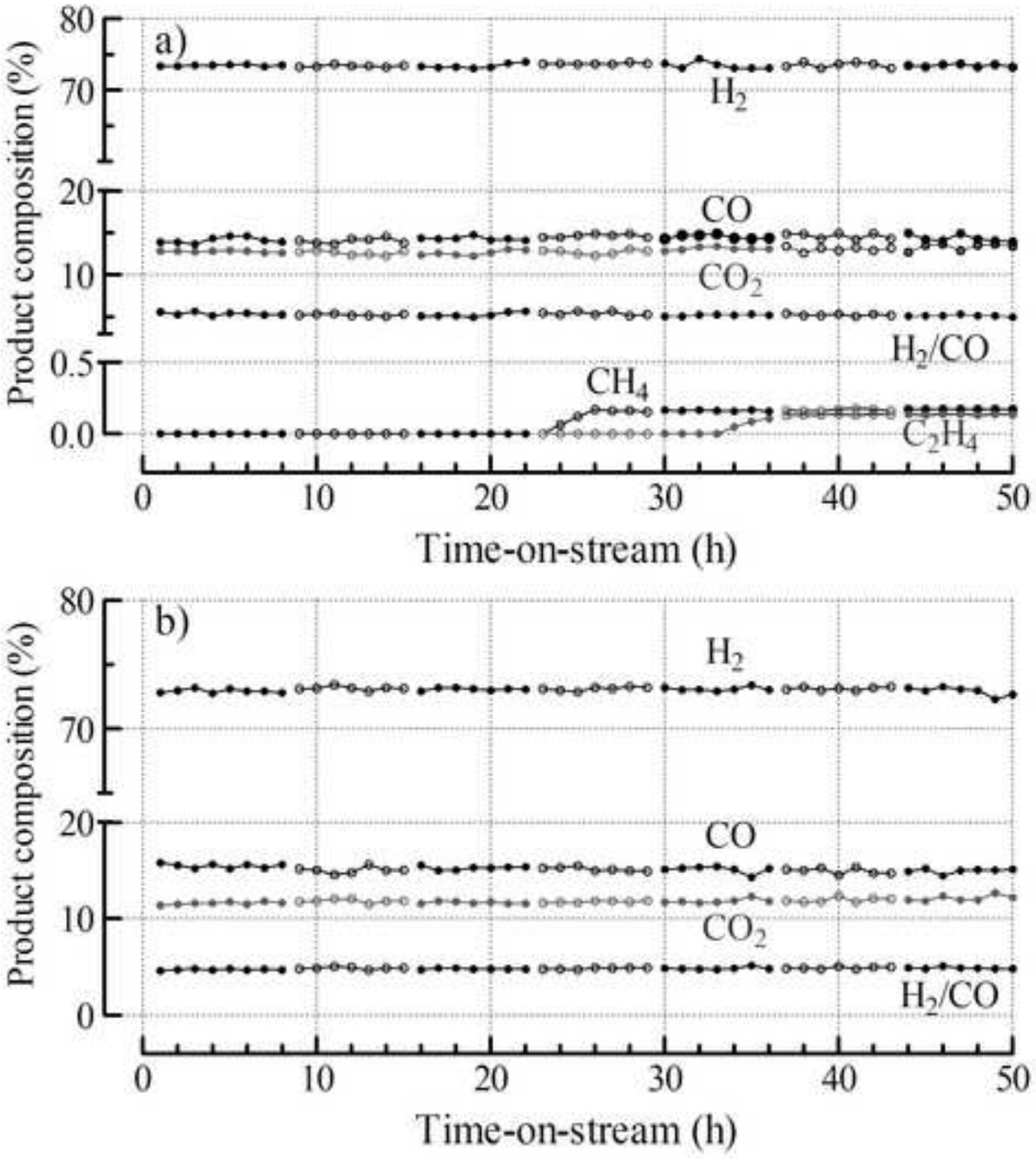

Figure 11 rev

Click here to download high resolution image

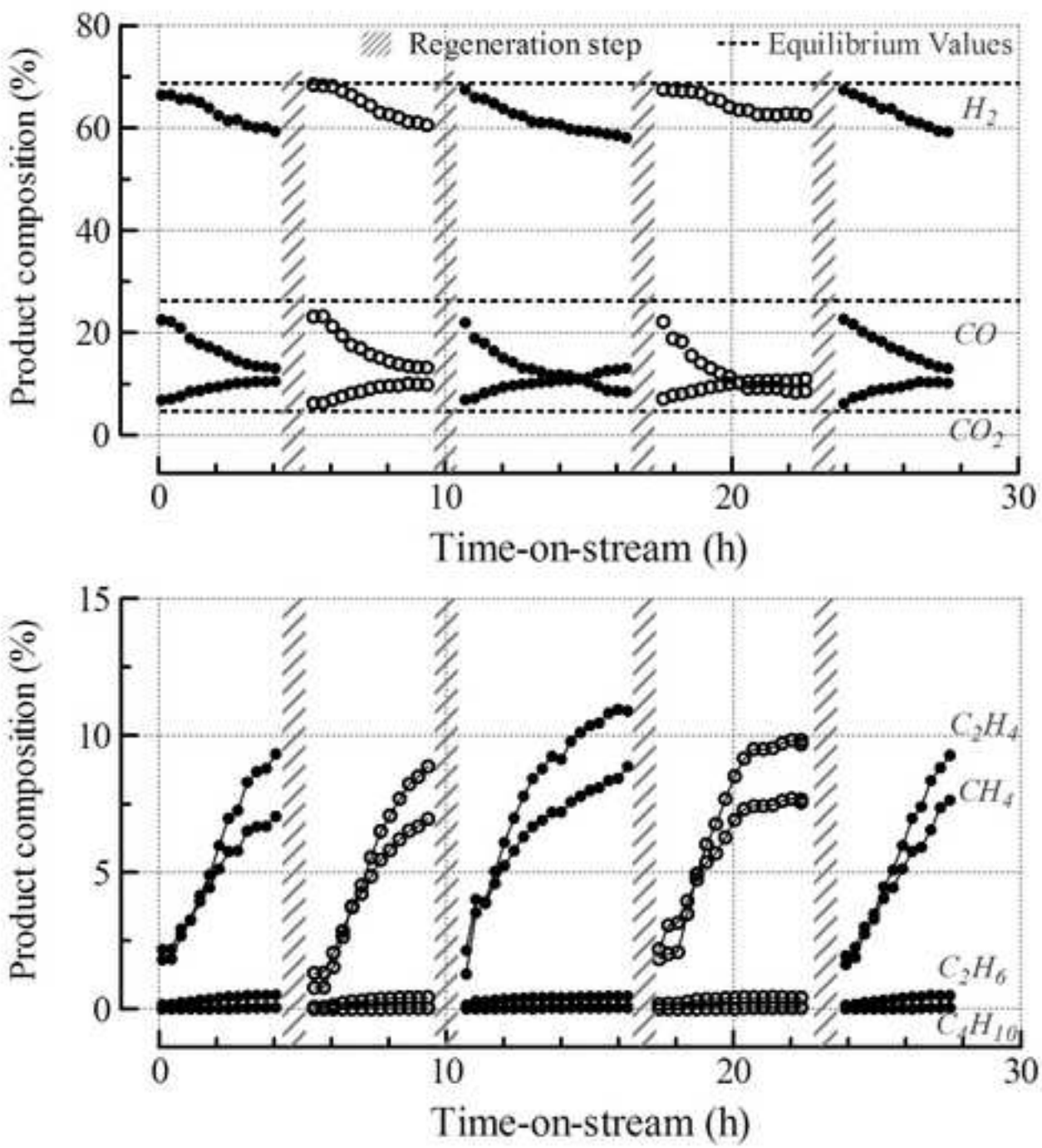

Figure 12 rev

Click here to download high resolution image

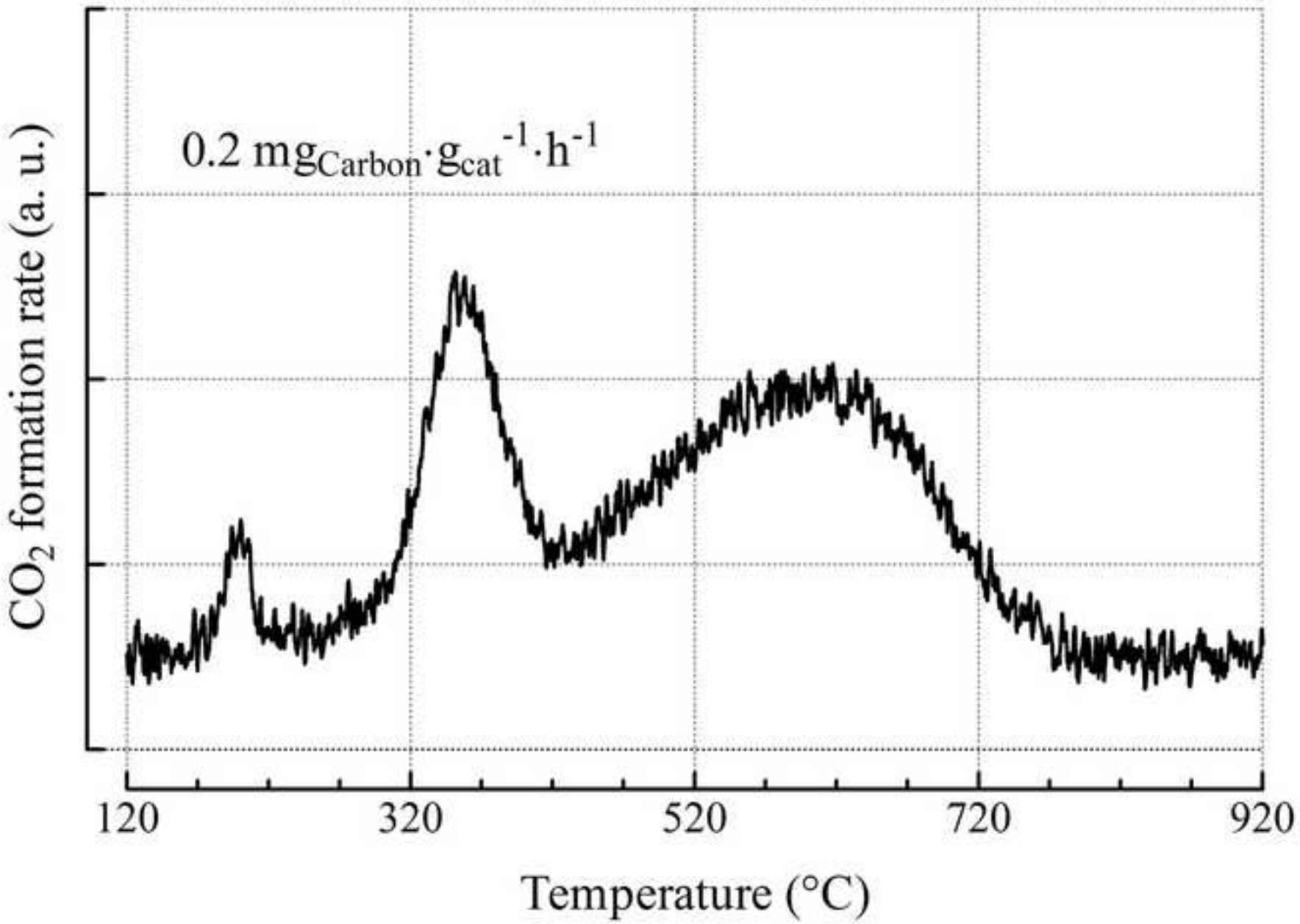

Figure 13 rev

Click here to download high resolution image

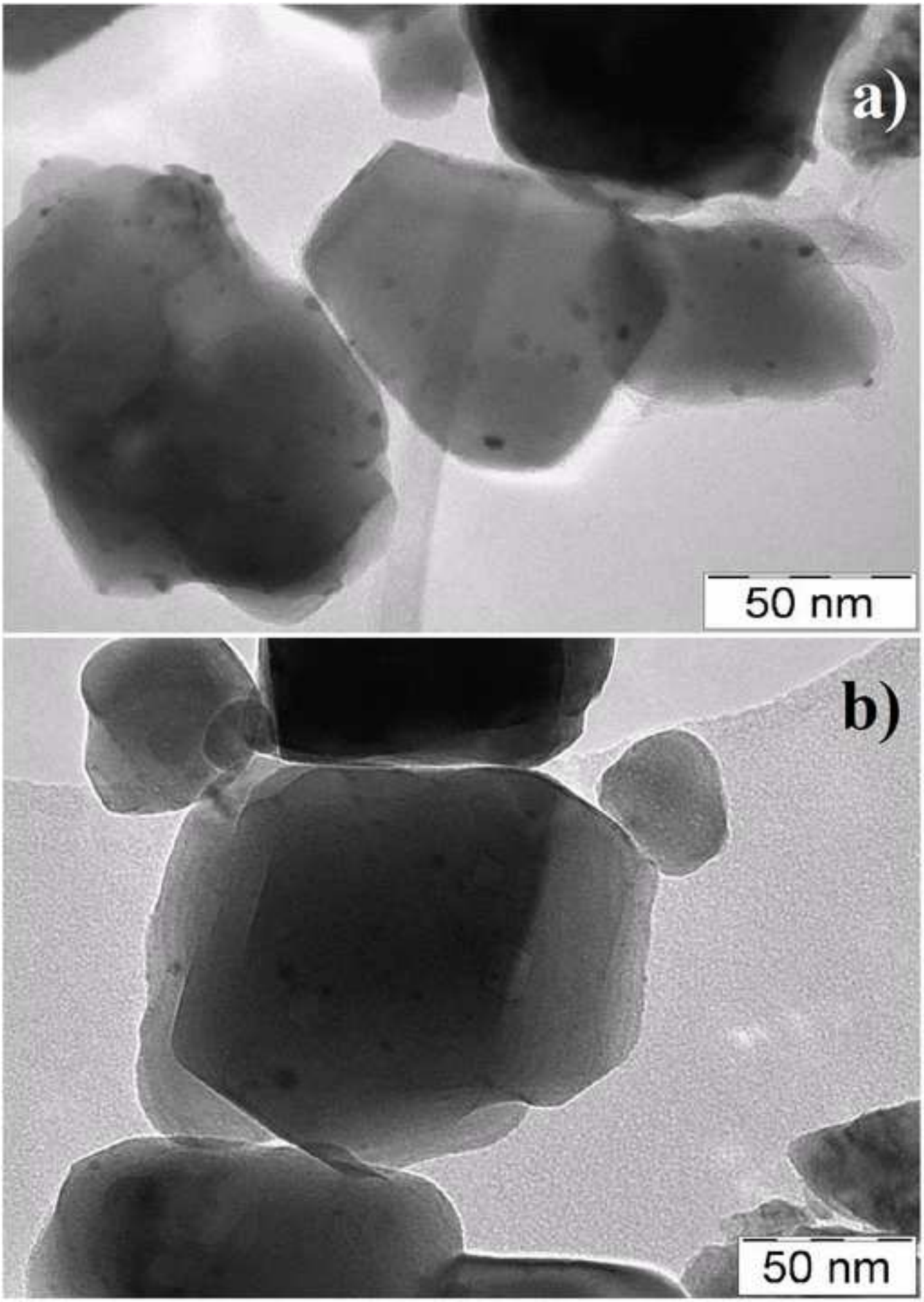

*Graphical Abstract

- Optimized temperature-controlled bed configuration:

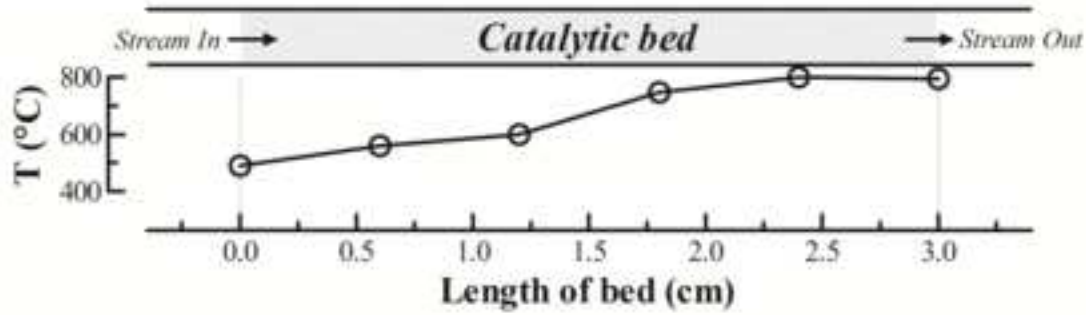

- Carbon/Coke minimization

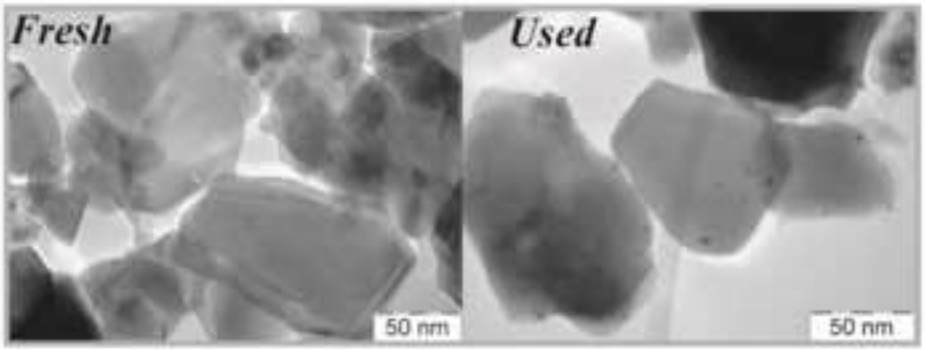

- Stable H_2-rich gas production

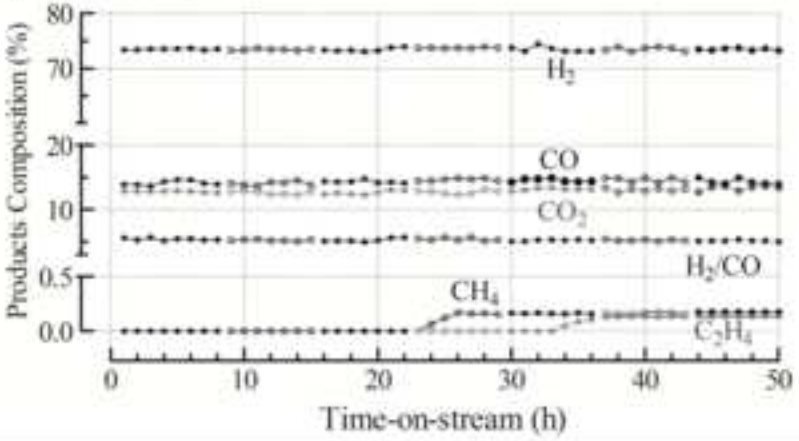

Highlights

- Well dispersed and small Pt particles in Pt/CeO_2 catalysts, especially 0.6-Pt/CeO_2 sample.
- Temperature-controlled bed configuration to avoid/minimize carbon/coke deposition due to cracking phenomena.
- High self-decoking activity with low noble metal content.
- High catalytic activity towards n-$C_{12}H_{26}$ SR over Pt/CeO_2 catalysts.
- Good stability of 0.6-Pt/CeO_2 system towards n-$C_{12}H_{26}$ SR reaction.

Hydrogen-rich gas production by steam reforming of n-dodecane.

Part I: Catalytic activity of Pt/CeO_2 catalysts in optimized bed configuration

Antonio Vita, Cristina Italiano, Concetto Fabiano, Lidia Pino, Massimo Laganà and Vincenzo Recupero

CNR-ITAE "Nicola Giordano", Via Salita S. Lucia sopra Contesse 5, 98126 Messina – Italy

*Corresponding author: antonio.vita@itae.cnr.it, Phone:+39090624297

Abstract

Onboard diesel reformer integrated with solid oxide fuel cell (SOFC) unit offers potential for high energy conversion efficiency and low emission levels on seagoing transport, avoiding cost associated with hydrogen storage and infrastructure. However, the development of active and stable liquid hydrocarbon-reforming catalyst still remains one of the major technological barriers for fuel-cell-based auxiliary power unit (APU) applications.

In this paper, the activity and stability of Pt/CeO_2 catalysts were investigated towards the steam reforming (SR) of n-dodecane, used as surrogate fuel for marine diesel. Pt-based catalysts (0.6-2.3 wt.% of metal loading) were prepared by Solution Combustion Synthesis (SCS) method and characterized by XRD, N_2-physisorption, CO-chemisorption, TPR, TPO and TEM techniques. Tests were performed at various process parameters, namely steam-to-carbon molar ratio (S/C=2-3), space velocity (GHSV=16,000-32,000 h^{-1}) and time-on-stream. An optimized temperature-controlled (500-800°C) bed configuration was adopted in order to avoid carbon/coke deposition due to n-dodecane cracking phenomena.

Superior chemical-physical properties of 0.6 wt.% Pt/CeO_2 system positively affect the SR performance. Pt-based catalyst showed catalytic activity comparable with that of the commercial Rh/ZDC (Rh/Zirconia-doped-Ceria). Total n-dodecane conversion and high H_2 concentration (73%, dry and N_2-free basis) were obtained at S/C=2.5 and GHSV=16,000 h^{-1}. Stable catalytic activity was found under start-up and shut-down cycles for 50 hours of time-on-stream. Restored catalytic performance was obtained under activity-regeneration cycles evaluated in more stressful conditions (S/C=1.5; GHSV=40,000 h^{-1}). This preliminary study was finalized to a diesel fuel processor design.

Keywords: hydrogen, diesel, n-dodecane, platinum-ceria catalyst, steam reforming.

1. Introduction

Energy generation in fuel cell (FC)-based auxiliary power units (APUs) is a very desirable option for both pollutants reduction and efficiency improvement in the transport sector [1,2]; the APU device, consisting of a fuel reformer, a cleanup system for reformate and a fuel cell stack, can provide energy for functions other than propulsion. APUs take advantage of liquid hydrocarbons (gasoline, diesel, kerosene) due to the easier storage and transportation compared to hydrogen, which is produced onboard; fuel cells used in APU systems include molten carbonate fuel cells (MCFCs), solid oxide fuel cells (SOFCs) and proton exchange membrane fuel cells (PEMFCs) [3]. The high temperature operation of SOFCs has the advantage of fuel flexibility: light hydrocarbons and CO can be used as fuels, avoiding the purification step (water gas shift and preferential oxidation or pressure swing adsorption) to obtain high purity hydrogen from syngas mixture [4]. SOFC-based APU systems, powered by the same type of fuel (diesel) used in the principal engine, are particularly interesting alternatives for supplying electrical energy to seagoing vehicles because can generate enough power for cabin comfort, to supply electricity for the refrigeration of load [5]. Diesel is the most used feedstock due to high energy density and existing fuel infrastructure [6].

Catalytic steam reforming (SR) of diesel can be considered the most important route for high hydrogen yield and high hydrogen concentration in the effluent gas [7]. Diesel fuel is a complex mixture of hydrocarbons (alkanes, cycloalkanes and aromatics, with carbon numbers ranging between 12 to 20) and sulfur compounds (alkylbenzothiophene and alkyldibenzothiopnene) [8]. In this study, n-dodecane ($C_{12}H_{26}$) was used as model compound for diesel fuel.

The highly endothermic SR of n-dodecane reaction (Eq. 1), with the simultaneous occurrence of water gas shift (WGS, Eq. 2) reaction:

$$C_{12}H_{26} + 12H_2O \rightarrow 12CO + 25H_2, \qquad \Delta H^{\circ}_{298} = 1866.5\ kJ \cdot mol^{-1} \tag{1}$$

$$CO + H_2O \leftrightarrow CO_2 + H_2, \qquad \Delta H^{\circ}_{298} = -41.1\ kJ \cdot mol^{-1} \tag{2}$$

proceeds on the catalyst surface by sequential steps forming lighter hydrocarbons that, in turn, react with steam, forming a mixture of H_2, CO and CO_2. However, due to the complexity of high-molecular-weight hydrocarbon reforming processes, numerous chemical reactions (i.e., methanation, thermal cracking, Boudouard and gasification,) can occur [9].

Carbon and coke deposition are major problems in reforming processes of high molecular weight hydrocarbon; this represents one of the major technological barriers that prevents the implementation of on-board liquid hydrocarbon reforming technology [10,11]. Coke is produced by thermal cracking of hydrocarbons, through the sequence reported in

Eq. 3, depending on the condition in which coke was formed: amorphous (filamentous) carbon is favored at low temperatures (<600°C) while graphitic (whisker) carbon is favored at high temperatures (>600°C) [12].

$$C_{12}H_{26} \rightarrow Olefins \rightarrow Polymers \rightarrow Coke \rightarrow Amorphous\ carbon \rightarrow Graphitic\ carbon \quad (3)$$

Carbon is produced by Boudouard reaction (Eq. 4), reverse gasification (Eq. 5) and hydrocarbons decomposition. Carbon forms can vary from whisker to filamentous depending on the operating conditions: Boudouard and reverse gasification reactions are favored at low temperatures, while hydrocarbons decomposition is favored at high temperatures [10,13].

$$2CO \rightarrow C + CO_2, \qquad \Delta H^{\circ}_{298} = -86.3\ kJ \cdot mol^{-1} \quad (4)$$

$$CO + H_2 \rightarrow C + H_2O, \qquad \Delta H^{\circ}_{298} = -130.4\ kJ \cdot mol^{-1} \quad (5)$$

Carbon and coke formation could cause degradation of the reformer performance and reduce its lifetime significantly. In a reformer system, there is a potential for carbon/coke formation in the catalytic reactor (reformer) as well as in its upstream and downstream units (i.e. vaporizer unit) [14]. Thus, there are several concerns for the design and operation of a reforming system for heavy hydrocarbon fuels [15]. One of the most crucial factors that influence the reforming performance is the uniform mixing between the reactants. As reported by Hartmann et al. [16], a not homogeneous mixture can be cause of hot spots, unwanted by-products formation and consequent carbon/coke deposition. Therefore, liquid fuels such as n-dodecane can be atomized and vaporized into microscopically sized droplets, while the overall reforming efficiency significantly improves by spraying the fuel with injection nozzles [17]. Porš et al. [18] and Pasel et al. [19] demonstrated that the long-term reforming performance could be improved by spraying the liquid fuel by twin fluid or swirl nozzle. An et al. [20] used a twin fluid nozzle to facilitate uniform mixing; they reported that reforming performance increased with shorter distance from the nozzle to the catalytic bed and larger mean drop size of fuel droplets. Alternatively, Koo et al. [21] demonstrated that a pre-reforming catalyst, installed after the gas-liquid spray nozzle, minimized the risk of carbon/coke formation due to the decomposition of the fuel. Xu et al. [22] investigated the reactants' inlet temperatures in order to avoid carbon formation inside the heating hose and to enhance the conversion efficiency.

The development of active and stable catalysts remains yet one of the major technological barriers for direct liquid hydrocarbon reforming at high temperature (800°C). Noble-metal-based catalysts (Pt, Rh, Pd, Ru) are more efficient because of their long-term activity and strong resistance to carbon [23-28]; besides, the presence of organic sulfur impurities in liquid hydrocarbons can affect the carbon deposition on reforming catalysts. Rh-based catalysts show higher sulfur tolerance than Pt, Ru and Ni catalysts during reforming reaction at 800°C [29]. Analogous trend was reported by Shekhawat et al. [30] towards n-tetradecane reforming in presence of sulfur. The effect of noble metal

catalysts supported on different supports (Al_2O_3, SiO_2, CeO_2 and MgO) was examined by Song and co-workers [31] in steam reforming of sulfur-containing liquid hydrocarbons (Norpar 13, Exxon Mobil). This systematic study confirms the high sulfur tolerance of Rh/Al_2O_3 catalyst in comparison with Ru, Pt and Pd samples on the same support; both Al_2O_3 and CeO_2 appear as promising supports for Rh, while CeO_2 emerges as the most adequate support for Pt.

The role of CeO_2 as promoter and/or support in catalysts formulation, due to its oxygen storage capacity (OSC), that can improve the reversibility of oxidation/reduction reactions of noble metals and the adsorption/dissociation of steam in catalyst surface increasing coke gasification, has been widely reported [32,33]. Our group has undertaken some studies on metal-supported CeO_2 catalysts prepared by combustion synthesis [34]; the derived strong metal-to-support interaction appears strictly related to the observed high catalytic activity and stability during hydrocarbons reforming. Moreover, the combustion synthesis provides an attractive practical alternative to the conventional preparation methods since is simple, low in cost, saving in time and energy consumption [33,34].

On this basis, the current investigation focuses the activity, stability and regenerability of Pt/CeO_2 catalysts, during steam reforming (SR) of n-dodecane, used as surrogate fuel for marine diesel. This preliminary study constitutes the first step of a more complete investigation (in progress) finalized to the development of a catalytic system for a diesel fuel reformer unit [35].

The Pt-based catalysts (0.6-2.3 wt.% of metal loading), prepared by Solution Combustion Synthesis (SCS) method, were characterized by XRD, N_2-physisorption, CO-chemisorption, TPR, TPO and TEM techniques. Tests were performed at various process parameters, namely steam-to-carbon molar ratio (S/C=2-3), space velocity (GHSV=16,000-32,000 h^{-1}) and time-on-stream. Results were compared with those of a commercial catalyst based on Rh/ZDC (Rh/Zirconia doped Ceria). An optimized temperature-controlled bed configuration (500-800°C) was developed in order to avoid carbon/coke deposition due to n-dodecane cracking phenomena.

2. Experimental Section

2.1. Catalysts Synthesis

Pt/CeO_2 catalysts were prepared by the Solution Combustion Synthesis (SCS) method, according to the procedure described elsewhere [36-38]. In a typical experiment, stoichiometric amount of Ce [$Ce(NO_3)_3$ from Sigma Aldrich] and Pt [H_2PtCl_6 from Sigma Aldrich] precursors with the suitable quantity of fuel [urea, CH_4N_2O from Alfa Aesar] were dissolved in a minimum quantity of water. The amount of catalyst precursors was adjusted in order to prepare samples with different platinum content, ranging between 0.6 wt.% and 2.3 wt.%. The amount of fuel was determined by the so-called fuel-to-oxidant ratio and it was calculated using the total oxidizing (O) and reducing (F) valences of the components in order to have an equivalence ratio equal to 1 (ϕ=O/F=1), that corresponds to the maximum release of

energy. The combustion mixture, gently aged in a quartz container of 600 cm^3 capacity until a homogeneous slurry was formed, was introduced into a preheated muffle furnace (350°C). At the beginning the slurry boils, foams and then undergoes intense flaming combustion with evolution of gases (N_2, CO_2, Cl_2 and H_2O), yielding a solid with a sponge form. The resulting powders were calcined at 600°C for 2 hours (heating rate set at 5°C·min^{-1}), pelletized, crushed and sieved to 200–600 μm for catalytic tests. The temperature profile during the combustion reaction was recorded using a thermocouple connected to a data acquisition unit; the related temperature-time profiles are shown in Figure 1. All the combustion reactions were characterized by an abrupt rise in temperature from 100°C (water boiling point) to the maximum value. The measured flame temperature (Figure 1) increased from 991 to 1263°C by increasing the platinum load from 0.6 wt.% to 2.3 wt.%; this was due to the different amount of mixed precursors and fuel that determine an increase of the heat released by the reaction. For comparison, the CeO_2 support was synthesized by the same route; in this case the flame temperature reached 535°C (not shown). Losses associated with conduction/convection phenomena and possible delay of the thermocouple signal, during the sudden change of the temperature could affect the recorded values. The Pt content in the catalytic powders was confirmed by chemical analysis (ICP/OES), as reported in Table 1.

2.2. Catalyst Characterization

The specific surface area, estimated from adsorption/desorption isotherms at liquid nitrogen temperature (-196°C) on a *Micromeritics ASAP 2020* instrument, was calculated according to the Brunauer-Emmet-Teller (BET) equation.

X-ray diffraction (XRD) analysis were done with a *Philips X-Pert 3710* diffractometer using a Cu Kα radiation at 40 kV and 20 mA. Diffraction patterns were recorded in the scan ranges of 2θ = 20°-75° (1.50°·min^{-1}) and 2θ = 27°-30° (0.06°·min^{-1}). The peaks were assigned according to the PCPFWIN database. The crystallite size was calculated by the Scherrer equation from the most intense CeO_2 (111) reflecting planes, while the CeO_2 lattice parameter (α) was derived from the related patterns at low scan rate.

The platinum dispersion was measured by CO-pulse chemisorption method proposed by Takeguchi et al. [39], using a *Micromeritics ChemiSorb 2750* instruments equipped with a TCD detector. A mixture of 10% CO in He was injected in pulses of 600 NμL each, until the fulfilment of constant outlet peaks. Before measurements all the catalysts were: i) reduced under pure H_2 flow (30 Nml·min^{-1}) for 30 min at 200°C; ii) oxidized under pure O_2 flow (30 Nml·min^{-1}) for 10 min at room temperature; iii) treated under CO_2 flow (30 Nml·min^{-1}) for 10 min at room temperature; iv) reduced under pure H_2 flow (30 Nml·min^{-1}) for 30 min at room temperature; with this method the CO adsorption on CeO_2, as carbonate species is avoided.

On the same apparatus, the reducibility of the catalysts was studied by H_2 temperature-programmed reduction (H_2-TPR). A continuous flow of 5% H_2/Ar (30 Nml·min^{-1}) followed over the catalyst and the temperature was raised from -

80°C up to 1000°C with a rate of 20°C·min^{-1}. Before measurements all the catalyst samples were treated in situ under pure O_2 flow for 30 min at 200°C. The H_2 consumption was monitored by a thermal conductivity detector (TCD) and the response was quantitatively calibrated from the TPR area of known amounts of CuO. The reduction degree of PtO_x samples was calculated from the ratio between the H_2 consumption to the theoretical H_2 required to reduce all the metal oxide.

O_2 temperature-programmed oxidation (O_2-TPO) was performed by using the same apparatus; the sample was pre-treated with He (30 Nml·min^{-1}) raising the temperature up to 1000°C with a rate of 20°C·min^{-1}. The CO_2 production was monitored by a quadrupole mass spectrometer (*QMS Thermo Scientific ProLab*); the response was quantitatively calibrated from the TPO area of known amounts of $CaCO_3$.

The morphology of fresh, used and regenerated catalysts was studied by Transmission Electron Microscopy (TEM) using a *Philips CM12* instrument. Specimens were prepared by ultrasonic dispersion of the powders in isopropyl alcohol then deposited on a holey copper grid.

2.3. Steam Reforming Experiments

The flow sheet and the main components of the test-rig employed in the present study are shown in Figure 2. Two HPLC pumps (*Agilent 1260 Infinity Binary Pump*) were used to inject fuel (n-dodecane, from Sigma Aldrich) and steam into separated vaporizers/mixers. H_2O was injected/gasified in the first evaporator maintained at 340°C and then transferred, using N_2 as carrier, to the second evaporator heated at 300°C in which n-dodecane was injected/gasified. High purity N_2 (99.999%, from Rivoira) was used in the experiments, keeping constant flow rate by using mass flow controllers (*Brooks Instrument Smart Mass Flow*). The mass balance (C, O and H) of the reactant mixture fed to the reactor (heated at 340°C) was used to determine the related evaporation degree; the complete vaporization, with mass balance values of ca. 99-101%, was derived. Similarly, a mass balance of 100±2% during all the catalytic experiments was obtained. The gaseous mixture was sent to the fixed-bed reactor (i.d.=0.6 cm), inserted into a furnace heated with a PID temperature controller. The pelletized catalyst (0.6g; 200–600 μm) diluted with 0.6 g of quartz particles (200–600 μm) was used in order to ensure an optimal temperature distribution through the catalytic bed. The catalysts were pre-reduced in situ with 50% H_2/N_2 stream at 200°C for 1 hour; then, the reactor was purged in N_2 flow and heated to the reaction temperature. The catalytic performances were measured at atmospheric pressure by 6 hours tests; at the end of the experiments the reactor was switched off and cooled down to room temperature under N_2 flow. Stability tests were performed over 50 hours of time-on-stream by sequential start-up and shut-down cycles of ca. 6 hours each. The reaction temperature was measured and controlled by three K-type chromel-alumel thermocouples. One thermocouple was positioned inside the catalytic bed to regulate the set temperature (T_{SET} = 800°C) with a temperature programmable

controller (*Omron, E5AK-TAA2005*), while the others two were kept at the inlet (T_{IN}) and at the outlet (T_{OUT}) of the catalytic bed. The effects of steam-to-carbon molar ratio (S/C = 2-3), space velocity (GHSV = 16,000-32,000 h^{-1}, as gas hourly space velocity of gases fed at 0°C and 1 bar per volume of catalyst) and platinum loading (Pt = 0.6-2.3 wt.%) on the activity of Pt/CeO_2 catalysts were evaluated. Additional tests were carried out at low steam-to-carbon molar ratio (S/C = 1.5) and high space velocity (GHSV = 40000 h^{-1}) under start-up and shut-down cycles, in order to observe the catalysts deactivation. After each cycle, the reactor was flushed with N_2 decreasing the temperature from 800°C to 25°C; then the regeneration process with air was done by re-increasing the temperature to 800°C. The CO_2 peak, revealed during this step, indicated the combustion of carbon deposits.

The product mixture was periodically analyzed (every 15 minutes) by an online Gas Chromatograph (*Agilent 5975C series 4C/MSD*) equipped with TCD and FID detectors and mass spectrometer. N_2 was used as internal standard for mass balance calibration. The catalytic activity was reported as n-dodecane conversion (X_{C12H26}), molar concentrations (on dry and N_2-free basis) of H_2, CO, CO_2, CH_4, by-products (C_2H_6, C_2H_4, C_3H_8, C_3H_6) and H_2/CO molar ratio. The experimental results were compared with the thermodynamic equilibrium values calculated by a commercial steady-state simulation package named *HSC Chemistry 7.1*®, based on the minimization of Gibbs free-energy of each of the existing species ($C_{12}H_{26}$, CH_4, H_2O, CO_2, CO, H_2, C-containing by-products and solid carbon). The calculation was carried out at the reaction temperature (T_{SET} = 800°C).

3. Results and Discussion

3.1. Catalysts Characterization

The main textural and structural characteristics of the synthesized Pt/CeO_2 catalysts, compared with the CeO_2 support, are reported in Table 1. Pt/CeO_2 samples exhibited specific surface areas varying in the range of 8-12 m^2/g, lower than 22 m^2/g obtained for the CeO_2; this could be due to the effect of flame temperature recorded during the combustion synthesis, higher with Pt/CeO_2 catalysts (991-1263°C) than with CeO_2 (535°C) [37,38]. XRD patterns of calcined CeO_2 sample and Pt/CeO_2 catalysts are shown in Figure 3, while the related CeO_2 crystallite sizes and lattice parameters are included in Table 1. All the systems were characterized by a typical cubic fluorite structure of ceria, corresponding to the (111), (200), (220), (311), (222), and (400) reflection planes. No clear evidence of Pt active phase could be noticed; this could be ascribed to the presence of small and well distributed particles or small amount not reveleable by diffraction. The average crystallite size of the samples, calculated by the Scherrer equation (Table 1), indicated particles size of 11.4 nm for the CeO_2 sample, that slightly increased to 23.7-27.1 nm for Pt/CeO_2 systems; this evidence could be related to the preparation methodology. As previously reported, morphological characteristics of combustion-synthesized powders are closely related to the nature of combustion, mainly combustion enthalpy and flame

temperature [37,38]. It is evident that lower flame temperatures (Figure 1) led to lower CeO_2 crystallite size (Table 1). Besides, as shown in Figure 3, ceria reflections of Pt/CeO_2 systems were slight shifted to higher degrees in comparison to those of pure CeO_2, in accordance with the lattice contraction reported in Table 1. Pt/CeO_2 lattice contraction (5.386-5.389 Å compared to 5.394 of CeO_2) indicated the partial incorporation of smaller Pt ions (Pt^{4+} ionic radius = 0.62 Å or Pt^{2+} ionic radius = 0.80 Å) into the lattice of ceria Ce^{4+} (Ce^{4+} ionic radius = 0.97 Å) to form a solid solution [40].

TEM micrographs of the studied catalysts are displayed in Figure 4, while the derived Pt particle sizes are reported in Table 1. As can be seen, all the catalysts appeared well dispersed with a narrow particle size distribution. Particularly, the 0.6-Pt/CeO_2 sample (Figure 4a) showed Pt particles ranging between 2-4 nm. At increasing Pt loading, the Pt particle size increased to 5-7 nm and 7-9 nm for 1.2-Pt/CeO_2 (Figure 4b) and 2.3-Pt/CeO_2 (Figure 4c) samples, respectively. Pt particle growth could depend on two different factors, namely higher Pt loading on the ceria surface and greater heat released during the solution combustion synthesis. Indeed, flame temperature (Figure 1) increased from 991°C to 1263°C with increasing platinum load, resulting in Pt particles growth due to the sintering phenomena. These evidences were in good agreement with the CO-chemisorption results reported in Table 1. The trend of Pt particle size in relation to the Pt loading is the same. As a consequence, 0.6-Pt/CeO_2 sample showed higher dispersion value (26.7%) than 1.2-Pt/CeO_2 (8.7%) and 2.3-Pt/CeO_2 (3.9%) catalysts.

Figure 5 compares the H_2-TPR profiles of CeO_2 and Pt/CeO_2 catalysts. The quantitative estimation of the reduction peaks, related only to the platinum species, is reported in Table 2. For bare ceria, two main reduction peaks were observed, at approximately 500 and 930°C, respectively. As reported in literature, the low-temperature peak is due to the reduction of CeO_2 surface oxygen, while the high-temperature peak is due to the reduction of CeO_2 bulk oxygen [36,41]. The presence of platinum induced significant modifications in the reduction profile, especially in the low temperature zone; the TPR patterns are divided into three temperature regions: region I (-80–20°C), region II (20–350°C) and region III (350–1020°C).

Region I could be associated to removal of the readily available surface oxygen adjacent to the metal, through a spillover mechanism; all catalysts presented a single and symmetric peak at sub-ambient temperature, that could be assigned to the reduction of well dispersed platinum oxide species with uniform particle size distribution [40,42]. The sub-ambient peak was shifted to higher temperature (Table 2) with increasing Pt loading. Moreover, hydrogen consumption could be correlated to the size of Pt oxide particles. Indeed, H_2 consumption increased from 0.6 to 1.1 $mmol_{H2}/g_{PtO2}$ with decreasing Pt loading from 2.25 to 1.13 wt.%, due to the presence of smaller PtO_x particles. However, further reduction of Pt content (0.57 wt.%) led to a decrease in hydrogen consumption (0.04 $mmol_{H2}/g_{PtO2}$). In this case, very small PtO_x particles were more affected by support and, consequently, could be reduced at higher temperature [42,43].

Region II could be correlated to the reduction of PtO_x interacting with the support and to the formation of Pt-Ce solid solution. Moreover, the contribution of CeO_2 surface reduction caused by H_2 spillover effect (especially 0.6 wt.% Pt/CeO_2 catalyst) cannot be excluded [40,44]. Indeed, hydrogen, after dissociation on metallic Pt, was able to spillover to CeO_2 and to reduce it at lower temperatures [45,46]. Hydrogen consumption decreased from 13.4 to 1.6 $mmol_{H2}/g_{PtO2}$ by increasing Pt loading from 0.57 to 2.25 wt.%. This could be due to different concomitant reasons, as well as the increase in platinum particle size and the decrease in Pt-Ce solid solution formation, as confirmed by XRD studies (Figure 3, Table 1). Moreover, 0.6 wt.% Pt/CeO_2 reduction profile in region II showed evident differences compared to the other samples. The broad peak in the range 30-300°C also contained the contribution of the reduction of Ce^{4+} ions adjacent to Pt species due to a spillover effect, because the amount of hydrogen consumption (13.4 $mmol_{H2}/g_{PtO2}$) was significantly higher than the nominal values [42,45,46].

Region III could be ascribed to CeO_2 bulk oxygen reduction, which was only slightly affected by Pt presence [47] and for this reason it is not quantified.

3.2. Non-Catalytic Experiments (Blank Tests)

One of the main problems that affect the catalyst performances during reforming of liquid hydrocarbon fuels is the deactivation by carbon/coke formation. The thermal cracking of long chain hydrocarbons as n-dodecane may result in the formation of a mixture of lower hydrocarbons that, in turn, could cause carbon or coke deposition [10,14,15]. Preliminary blank tests were carried out in order to determine the temperature range inside where n-dodecane cracking reaction could occur. Figure 6a shows the scheme of the model reactor (quartz tube and furnace) for in-situ measurements of the temperature profile along the quartz tube. The temperature (T_C) was controlled by one K-type chromel-alumel thermocouple centered within the quartz reactor, while other six thermocouples were positioned along the reactor to measure the temperatures (T1, T2, T3, T4, T5, T6) between the inlet and the outlet (Figure 6a). Blank tests were carried out varying temperature (T_C = 400-700°C) at S/C = 2, with a total mixture ($C_{12}H_{26}$, N_2, H_2O) flow equal to 100 $Nml \cdot min^{-1}$, without catalyst. Temperature profiles for each test were registered and associated with the formation of visible carbon inside the reactor and with the ethylene formation revealed by the GC/MS analysis of the outlet products. Tests results, reported in Figure 6b, indicated that carbon deposition and ethylene formation were observed at temperatures higher than 550°C. Thus, n-dodecane cracking could occur at temperatures higher than 550°C.

Based on the obtained results, a bed configuration with an optimized temperature-control (Figure 6c) was adopted for catalytic tests, in order to avoid/minimize carbon formation due to cracking phenomena, especially at the inlet of the catalytic bed. The position of the catalytic bed within the furnace was determined in order to have an opportune temperature gradient between the inlet and the outlet (Figure 6c). Figure 6d shows the temperature profile recorded

during a catalytic test carried out at T_{SET} = 800°C, S/C = 2, GHSV = 24,000 h^{-1} with 1.2-Pt/CeO_2 catalyst. With this configuration, the temperature of the catalytic bed increased from 490 (T_{IN}) to 800°C (T_{SET}). Thus, the inlet temperature (490°C) remained lower than the cracking ignition temperature (550°C), avoiding the thermal cracking in the front part of the catalytic bed. However, a partial decomposition of n-dodecane into short-chain hydrocarbons (C1 – C11) probably occurred in the first part of the bed at lower temperature; these hydrocarbons could then be converted in the second part of catalytic bed at higher temperatures.

3.3. Catalytic Activity

3.3.1. Influence of steam-to-carbon molar ratio on the activity of the 1.2-Pt/CeO_2 catalyst

Figure 7 shows the influence of steam-to-carbon molar ratio (S/C = 2-3) on the activity of the 1.2-Pt/CeO_2 catalyst towards n-dodecane SR at T_{SET} = 800°C and GHSV = 24,000 h^{-1}. Results are reported in terms of n-dodecane conversion (X_{C12H26}) and product concentrations (H_2, CO, CO_2, CH_4 and C_2H_4, on dry and N_2-free basis). Experimental results are compared to thermodynamic equilibrium values, calculated at 800°C. It can be seen that n-dodecane conversion was total at all the investigated S/C molar ratios. The results showed that the increase of S/C ratio did not have an evident effect on the catalyst performance. H_2 concentration slightly increased from 70.7 to 71.7%, while almost constant CO (14.8-15.1%) and CO_2 (12.8-13.4%) concentrations were recorded in all the investigated S/C range. Constant traces of CH_4 (ca. 0.4%) and C_2H_4 (ca. 0.2%) were also revealed. The presence of other hydrocarbons that fell below the detection limits (< 0.05%) could not be excluded.

It is clearly evident that CO and CO_2 concentrations differed from equilibrium values. In particular, products mixture contained lower amount of CO and higher amount of CO_2 compared to the thermodynamic composition at all the studied S/C molar ratio. Besides, H_2O conversion (69.9-49.7%) resulted higher than equilibrium values (62.6-46.9%). This was mainly due to the temperature gradient present along the catalytic bed and described on section 3.2, while the thermodynamic predicted values were derived at 800°C. Indeed, the temperature along the catalytic bed increased from 480 (T_{IN}) to 800°C (T_{SET}), suggesting that the contributions of WGS (Eq. 2) and methanation reactions ($CO+3H_2 \rightarrow CH_4+H_2O$, $\Delta H°_{298}$=-206.2 kJ·mol^{-1} and $CO_2+4H_2 \rightarrow CH_4+2H_2O$, $\Delta H°_{298}$=-165.0 kJ·mol^{-1}) were more relevant than the predictable values (at 800°C) [48]. Whereby, the exothermic WGS and methanation reactions could be favored in the first part of the bed at lower temperature, inducing a low CO concentration and, consequently, a high H_2/CO (4.7-4.8) molar ratio, a high CO_2 concentration and a more high CH_4 content in the reformate.

Because steam prevents carbon/coke formation but, at the same time, requires more energy, S/C = 2.5 was selected for subsequent investigation, constituting a good compromise between catalytic and energetic efficiency of the related fuel processor.

3.3.2. Influence of space velocity on the activity of the1.2-Pt/CeO_2 catalyst

The effect of space velocity (GHSV = 16,000-32,000 h^{-1}) on the catalytic activity of 1.2-Pt/CeO_2 catalyst was investigated at T_{SET} = 800°C and S/C = 2.5. Results are shown in Figure 8, highlighting almost stable catalytic activity at all investigated GHSVs. However, the1.2-Pt/CeO_2 system showed higher performance at 16,000 h^{-1}, in terms of total fuel conversion (maintained also at 24,000 h^{-1}), higher hydrogen production (72.8%) and absence of by-products (CH_4, C_2H_6, C_2H_4), associated with a H_2/CO molar ratio of 4.8. Increasing the GHSV up to 32,000 h^{-1}, the catalytic activity slightly decreased as n-dodecane conversion (98.8%) and H_2 concentration (70.0%), while the amount of by-products slightly increased (CH_4=1.2%, C_2H_6=0.2%, C_2H_4=1.1%). Also in this case, the temperature gradient along the catalytic bed played a key role in determining final products concentration, with CO (14.7-15.2%) and CO_2 (12.0-13.0%) concentrations respectively lower and higher than equilibrium values (19.2% for CO and 10.0% for CO_2).

The slight loss of activity, recorded by increasing space velocity, could be due to different causes: n-dodecane steam reforming is a strongly endothermic reaction often limited by heat and mass transfer, especially in packed bed reactors [49,50]. These phenomena enhanced at higher space velocity, could contribute to the decrease of the catalytic performance. In addition, cold spots in the reactor cannot be excluded, due to high steam amount through the reactor [51]. Besides, the increase in the GHSV implied a short residence time of reagents on the surface active sites; this could be not sufficient to maintain the activity of the samples considering the low dispersion of Pt particles (8.7%, measured by chemisorption analysis). Whereby, GHSV ranging between 16,000 and 24,000 h^{-1} appeared to be a favourable option for n-dodecane steam reforming.

3.3.3. Influence of platinum loading on the activity of Pt/CeO_2 catalysts

Figure 9 shows the influence of platinum loading (0.6-2.3 wt.%) on the catalytic activity of the Pt/CeO_2 catalyst towards n-dodecane SR at T_{SET} = 800°C, S/C = 2.5 and GHSV = 24,000 h^{-1}. Although n-dodecane conversion was almost total for all the prepared catalysts, the H_2 concentration slightly decreased from 71.7 to 68.8% by increasing the platinum loading from 0.57 to 1.13 wt.%. Indeed, the increase of noble metal content did not positively affect the catalyst performance. Particularly, 0.57 wt % Pt/CeO_2 system showed total n-dodecane conversion and higher H_2 concentration (71.7%) in absence of by-products. Increasing noble metal loading up to 1.13 wt.%, n-dodecane conversion still remained complete, H_2 concentration slightly decreased to 71.4%, but low concentrations of CH_4 (0.4%) and C_2H_4 (0.3%) were detected. A further increase in Pt loading (2.25 wt.%) led to a decrease of the catalytic performance: the H_2 concentration decreased to 68.8% and the content of by-products increased (CH_4=2.1%,

C_2H_6=0.2%, C_2H_4=2.8%); in addition, the presence of other hydrocarbons (> C2) below the detection limit (< 0.05%) could not be excluded.

The low activity of the sample with high metal loading was probably related to physico-chemical and morphological properties of the catalysts. As reported in Table 1, the increase in platinum loading led to the decrease of metal dispersion (from CO-chemisorption) and the increase of Pt particle size (from TEM). As previously mentioned this behaviour could be related to the adopted solution combustion method and, particularly, to the heat released during the synthesis. The presence of larger Pt metal grains for 1.13 wt.% Pt/CeO_2 and especially for 2.25 wt.% Pt/CeO_2 systems led to the decrease of the catalytic performances. Moreover, higher Pt loadings could lead to the formation of multiple adjacent active sites promoting, in turn, additional coking, responsible for catalyst deactivation.

Conversely, the 0.6 wt.% Pt/CeO_2 system showed higher catalytic activity due to the presence of small and homogeneously distributed Pt particles on the ceria support.

3.4. Stability Tests

3.4.1. Time-on-stream experiments

Figure 10a shows the performance of 0.6-Pt/CeO_2 catalyst towards n-dodecane SR T_{SET} = 800°C, S/C = 2.5 and GHSV = 16,000 h^{-1} during 50 hours of time-on-stream. Stability tests were carried out with successive start-up and shut-down cycles of ca. 6 hours each. Moreover, catalytic performance of commercial Rh/ZDC (Rh/Zirconia-doped-Ceria) catalyst was also reported in Figure 10b as comparison. The aim of this test was to investigate carbon/coke formation phenomena, highlighting the applicability of the optimized temperature-controlled bed configuration (Figure 6), designed and implemented to overcome one of the major problems related to reforming of liquid hydrocarbons reforming [10]. The 0.6-Pt/CeO_2 catalyst showed good and stable performances in terms of total n-dodecane conversion (not reported) and H_2 concentration (ca. 73%). No relevant deactivation of the catalyst was observed throughout 50 hours of reaction, but low production of CH_4 (ca. 0.2%) and C_2H_4 (ca. 0.1%) was envisaged after 24 and 34 hours of test, respectively. In addition, the Pt-based system (Figure 10a) showed catalytic activity and stability similar to that of commercial Rh-based system (Figure 10b). The low amount and cost of the Pt sample (0.6 wt.% of Pt), related to the commercially available Rh-based catalyst (2.0 wt.% of Rh), can make it as a promising catalyst for diesel reforming.

The regeneration ability of the catalyst was evaluated during further tests carried out at lower steam-to-carbon molar ratio (S/C = 1.5) and higher space velocity (GHSV = 40,000 h^{-1}) under sequential start-up and shut-down cycles. In this conditions, as evidenced in Figure 11, the performance of the catalyst decreased: the H_2 and CO concentration in the reformate gases decreased during the first 5h of test; while a progressive increase in the CO_2 and by-products

concentration could be observed. After the regeneration step with air, the initial gas concentration in the reformate was restored, indicating that the full regeneration of the catalyst is possible.

Promising activity of the 0.6 wt.% Pt/CeO_2 catalyst could be associated to different contributions. The adopted catalytic bed configuration allowed avoiding/minimizing carbon/coke formation, especially at the inlet of the catalytic bed. Besides, the use of ceria as support played another significant role in SR of n-dodecane. The principal role of ceria was connected with the ability to increase the adsorption of steam by its vacant oxygen and to transfer oxygen to the supported metallic site, keeping the surface relatively free of carbon. This self-decoking capability of ceria-based catalysts, due to the gasification reaction by oxygen species from the lattice, was previously studied and discussed by other authors [52-55] and also in our previous papers [34,36,40,56,57]. In addition, partial incorporation of Pt ions into the ceria matrix to form Pt-Ce solid solution (as revealed from XRD and TPR analysis) enhanced oxygen mobility by increasing CeO_2 structural defects. This further limited carbon deposition on the catalyst surface. Moreover, small particles were determined for 0.6 wt.% Pt/CeO_2 catalyst (TEM analysis). As reported in literature, coke and carbon (graphite or filamentous) carbon involves the formation of C–C bonds on multiple atoms sites, resulting structure-sensitive, i.e. sensitive to surface structure and metal crystallite size [58,59]. Bitter et al. [60] found that catalysts containing larger Pt crystallites deactivated more rapidly than those containing small crystallites. The 0.6-Pt/CeO_2 catalyst constituted a promising catalytic system for n-dodecane SR reaction.

3.4.2. Characterization of 0.6-Pt/CeO_2 used-regenerated catalyst

Figure 12 shows the TPO profile of the used 0.6-Pt/CeO_2 catalyst after the stability test. The analysis evidenced a carbon formation rate equal to 0.2 $mg_{carbon} \cdot g_{cat}^{-1} \cdot h^{-1}$ (corresponding to ca. 0.7 wt.%), suggesting good carbon resistance after 50 hours of time-on-stream. Several CO_2 peaks were observed, indicating different types of carbonaceous species with different reactivity toward oxidation. Contrarily, no peaks were found in the TPO profile of the commercial catalyst (not shown). As reported in Rostrup-Nielsen's review [7], three types of carbon were identified on steam reforming catalysts: i) pyrolitic (derived from thermal cracking of hydrocarbons at temperatures higher than 597°C and low S/C ratios); ii) filamentous (produced at temperatures above 447°C and low S/C ratios); iii) encapsulating (non reactive film with C-H bonds produced through polymerization at temperatures below 497°C and low S/C ratios). The formation of these carbon species was influenced by several parameters, such as catalyst (surface properties), feed composition (hydrocarbon, S/C ratio) and reaction temperature. As shown in Figure 11, low-temperature peaks (195 and 350°C) could be associated to the formation of soft or surface sensitive carbon deposits [61,62]. A widely accepted interpretation of these peaks is that they correspond to more reactive carbon or species located at metal/support interfaces [63,64]. The large CO_2 peak at ca. 605°C could be associated to pyrolitic carbon, formed by

cracking/decomposition of n-dodecane or low chain hydrocarbons [61,65]. Some authors suggested that this peak corresponds to less reactive carbon species deposited on the support [63-65].

Figure 13 shows the TEM images of the used and regenerated 0.6-Pt/CeO_2 catalysts. By comparing the TEM micrographs of fresh (Figure 4a) and used-regenerated samples, the morphological structure of the catalyst did not show any relevant changes. After stability test, Pt particles appeared small and well distributed with size ranging from 2.5 to 4.5 nm (Figure 13a). Moreover, only traces of carbon deposition were noticed. The absence of severe particles aggregation on spent catalysts denoted that metal sintering on the support surface was not a dominant phenomenon under the investigated conditions, which is in agreement with the good catalytic performances recorded during the 50 hours of time-on-stream. Moreover, TEM image of the regenerated system (Figure 13b) showed that the regeneration process carried out to remove carbon deposited during the reforming process, did not affect the size of platinum particles (2-5 nm), signal of a good resistance to metal sintering of the studied catalyst.

3.5. Conclusions

In this study, catalytic activity of Pt/CeO_2 catalysts (0.6-2.2 wt% of metal loading) was probed towards steam reforming of n-dodecane, as model compound of marine diesel. The effect of steam-to-carbon molar ratio (S/C = 2-3), space velocity (GHSV = 16,000-32,000 h^{-1}) and time-on-stream were also evaluated. Catalysts were prepared by solution combustion synthesis (SCS) and characterized by XRD, N_2-physisorption, CO-chemisorption, TPR, TPO and TEM techniques. Between the prepared catalysts, 0.6-Pt/CeO_2 sample showed high catalytic activity in terms of total n-dodecane conversion and high H_2 concentration (ca. 73%, dry and N_2-free basis) at T_{SET} = 800°C, S/C = 2.5 and GHSV = 16,000 h^{-1}. The Pt-based catalyst showed stable performance during 50 hours of reaction, with an activity similar to that of a commercial Rh-based system.

A special bed configuration with an adequate temperature control allowed limiting/avoiding carbon/coke formation due to n-dodecane cracking phenomena, especially at the inlet of the catalytic bed. Temperature gradient (ca. 480-800°C) along the catalytic bed played a key role in determining final products concentration due to the occurrence of WGS equilibrium reaction.

Physico-chemical and morphological properties of the 0.6-Pt/CeO_2 sample catalyst further limited carbon deposition on the catalyst surface, making it a promising active and stable system for n-dodecane steam reforming reaction.

Acknowledgements

This work was funded by the Italian Ministry of Education, University and Research, MIUR. “PON Ricerca e Competività”, in the framework of the “TESEO” (High Efficiency Technologies for Energy and Environmental Sustainability On-board) project.

References

[1]. R.C. Samsun, J. Pasel, R. Peters, D. Stolten, Int. J. Hydrogen Energy 40 (2015) 6405–6421.

[2]. A.V. González, L.J. Pettersson, Catal. Today 210 (2013) 19–25.

[3]. T. Aicher, B. Lenz, F. Gschnell, U. Groos, F. Federici, L. Caprile, L. Parodi, J. Power Sources 154 (2006) 503–508.

[4]. S.Y. Jung, D.G. Ju, E.J. Lim, S.C. Lee, B.W. Hwang, J.C. Kim, Int. J. Hydrogen Energy 40 (2015) 13412–13422.

[5]. G. Dolanc, B. Pregelj, J. Petrovčič, J. Pasel, G. Kolb, J. Power Sources 313 (2016) 223–232.

[6]. R.R. Kondakindi, A. Kundu, K. Karan, B.A. Peppley, A. Qi, C. Thurgood, P. Schurer, Appl. Catal. A 390 (2010) 271–280.

[7]. J.R. Rostrup–Nielsen, Catalytic steam reforming, in: J.R. Anderson, M. Boudart (Eds), Catal. Sci. Technol., vol. 5, Springer–Verlag, Berlin, 1984.

[8]. X. Xu, P. Li, Y. Shen, Appl. Energy 108 (2013) 202–217.

[9]. C.H. Bartholomew, Catal. Rev. Sci. Eng. 24 (1982) 67–112.

[10]. R.D. Parmar, A. Kundu, K. Karan, J. Power Sources 194 (2009) 1007–1020.

[11]. I.E. Achouri, N. Abatzoglou, C. Fauteux–Lefebvre, N. Braidy, Catal. Today 207 (2013) 13–20.

[12]. D. Shekhawat, D.A. Berry, T.H. Gardner, J.J. Spivey, in: J.J. Spivey, K.M. Dooley (Eds), Catalysis 19 (2006) 184–253.

[13]. I. Chen, D.–M. Shiue, Ind. Eng. Chem. Res. 27 (1988) 1391–1396.

[14]. X. Xu, P. Li, Y. Shen, Appl. Energy 108 (2013) 202–217.

[15]. Y. Chen, H. Xu, Y. Wang, X. Jin, G. Xiong, Fuel Process. Technol. 87 (2006) 971–978.

[16]. L. Hartmann, K. Lucka, H. Köhne, J. Power Sources 118 (2003) 286–297.

[17]. B. Lindström, J.A.J. Karlsson, P. Ekdunge, L. De Verlier, B. Häggendal, J. Dawody, M. Nilsson, L.J. Pettersson, Int. J. Hydrogen Energy 24 (2009) 3367–3381.

[18]. Z. Porš, J. Pasel, A. Tschauder, R. Dahl, R. Peters, D. Stolten, Fuel Cells 8 (2008) 129–137.

[19]. J. Pasel, J. Meibner, Z. Porš, R.C. Samsun, A. Tschauder, R. Peters, Int. J. Hydrogen Energy 32 (2007) 4847–4858.

[20]. S.M. An, Sang, W.S. Kim, S.Y. Lee, Int. J. Hydrogen Energy 36 (2011) 5342–5349.

[21]. K.Y. Koo, M.G. Park, U.H. Jung, S.H. Kim, Int. J. Hydrogen Energy 39 (2014) 10941–10950.

[22]. X. Xu, S. Zhang, P. Li, Int. J. Hydrogen Energy 39 (2014) 19593–19602.

[23]. A. Azad, M.J. Duran, Appl. Catal. A 330 (2007) 77–88.

[24]. A. Azad, M.J. Duran, A.K. McCoy, M.A. Abraham, Appl. Catal. A 332 (2007) 225–236.

[25]. J.T. Richardson, M. Garrait, J. Hung, Appl. Catal. A 255 (2003) 69–82.

[26]. M. Ferrandon, T. Krause, Appl. Catal. A 311 (2006) 135–145.

[27]. M. Ferrandon, A.J. Kropf, T. Krause, Appl. Catal. A 379 (2010) 121–128.

[28]. A.F. Ghenciu, Curr. Opin. Solid State Mater. Sci. 6 (2002) 389–399.

[29]. U. Hennings, R. Reimert, Appl. Catal. B 70 (2005) 498–508.

[30]. D. Shekhawat, T.H. Gardner, D.A. Berry, M. Salazar, D.J. Haynes, J.J. Spivey, Appl. Catal. A 311 (2006) 8–16.

[31]. C. Xie, Y. Chen, M.H. Engelhard, and C. Song, ACS Catal. 2 (2012) 1127–1137.

[32]. H.M. Li, Q.C. Zhu, Y.L. Li, M.C. Gong, Y.D. Chen, J.L. Wang, Y.Q. Chen, J. Rare Earths 28 (2010) 79–84.

[33]. A. Trovarelli, Catal. Rev.-Sci. Eng. 38(1996) 439–520.

[34]. L. Pino, A. Vita, F. Cipitì, M. Laganà, V. Recupero, Appl. Catal. A 306 (2006) 68–77.

[35]. C. Fabiano, C. Italiano, A. Vita, L. Pino, M. Laganà, V. Recupero, HYdrogen POwer Theoretical and Engineering Solutions International Symposium 2015, Toledo, Spain

[36]. L. Pino, A. Vita, F. Cipitì, M. Laganà, V. Recupero, Appl. Catal. B 104 (2011) 64–73.

[37]. C. Italiano, A. Vita, C. Fabiano, M. Laganà, L. Pino, Int. J. Hydrogen Energy 40 (2015) 11823–11830.

[38]. A. Vita, C. Italiano, C. Fabiano, M. Laganà, L. Pino, Mater. Chem. Phys. 163 (2015) 337–347.

[39]. T. Takeguchi, S. Manabe, R. Kikuchi, K. Eguchi, T. Kanazawa, S. Matsumoto, W. Ueda, Appl. Catal. A 293 (2005) 91–96.

[40]. L. Pino, A.Vita, M. Cordaro, V. Recupero, M. S. Hegde, Appl. Catal. A 243 (2003) 135–146.

[41]. J. Xiaoyuan, L. Guanglie, Z. Renxian, M. Jianxin, C. Yu, Z. Xiaoming, Appl. Surf. Sci. 173 (2001) 208–220.

[42]. H.-H. Liu, Y. Wang, A.-P. Jia, S.-Y. Wang, M.-F. Luo, J.-Q. Lu, Appl. Surf. Sci. 314 (2014) 725–734.

[43]. S.K. Meher, M. Cargnello, H. Troiani, T. Montini, G.R. Rao, P. Fornasiero, Appl. Catal. B 130 (2013) 121–131.

[44]. Z. He, X. Wang, Y. Pu, Z. Qian, Int. J. Hydrogen Energy 37 (2012) 11132–11140.

[45]. Y. Ji, A.M.J. van der Eerden, V. Koot, P. J. Kooyman, J.D. Meeldijk, B.M. Weckhuysen, D.K.C. Koningsberger, J. Catal. 234 (2005) 376–384.

[46]. T. Hou, B. Yu, S. Zhang, T. Xu, D. Wang, W. Cai, Catal. Commun. 58 (2015) 137–140.

[47]. S. Damyanova, B. Pawelec, K. Arishtirova, M.V. Martinez Huerta, J.L.G. Fierro, J.L.G. Fierro, Appl. Catal. B 89 (2009) 149–159.

[48]. R.A. Dagle, A. Karim, G. Li, Y. Su, D.L. King, Syngas conditioning, in: D. Shekhawat, J.J. Spivey and D.A. Berry (Eds.), Fuel cells: Technologies for fuel processing, Elsevier, 2011, pp. 361–408.

[49]. A. Vita, G. Cristiano, C. Italiano, L. Pino, S. Specchia, Appl. Catal. B 162 (2015) 551–563.

[50]. J.M. Bae S. Ahmed, R. Kumar, E. Doss, J. Power Sources 139 (2005) 91–95.

[51]. S. Martin, A. Wörner, J. Power Sources 196 (2011) 3163–3171.

[52]. M.D. Salazar-Villalpando, D.A. Berry, T.H. Gardner, Int. J. Hydrogen Energy 33 (2008) 2695–2703.

[53]. M. Salazar, D.A. Berry, T.H. Gardner, D. Shekhawat, D. Floyd, Appl. Catal. A 310 (2006) 54–60.

[54]. K. Tomishige, T. Kimura, J. Nishikawa, T. Miyazawa, K. Kunimori, Catal. Commun. 8 (2007) 1074–1079.

[55]. G. Nahar, V. Dupont, Renew. Sust. Energ. Review 32 (2014) 777–796.

[56]. L. Pino, A. Vita, F. Cipitì, M. Laganà, V. Recupero, Catal. Lett. 122 (2008) 121–130.

[57]. A. Vita, L. Pino, F. Cipitì, M. Laganà, V. Recupero, Fuel Process. Technol. 127 (2014) 47–58.

[58]. M.L. Toebles, J.H. Bitter, A.J. Van Dillen, K.P. de Jong, Catal. Today 76 (2002) 33–42.

[59]. K. Tao, S. Lei, Q. Ma, D. Wang, C. Zeng, C. Kong, M. Wu, L. Chen, S. Zhou, Y. Hu, N. Tsubaki, Chem. Eng. J. 221 (2013) 25–31.

[60]. J.H. Bitter, K. Seshan, J.A. Lercher, J. Catal. 183 (1999) 336–343.

[61]. B. D. Gould, X. Chen, J. W. Schwank, Appl. Catal. A 334 (2008) 277–290.

[62]. T.A. Westrich, X. Chen, J.W. Appl. Catal. A 386 (2010) 83–93.

[63]. A. Tanksale, J.N. Beltramini, J.A. Dumesic, G.Q. Lu, J. Catal. 258 (2008) 366–377.

[64]. A. Shamsi, J.P. Baltrus, J.J. Spivey, Appl. Catal. A 293 (2005) 145–152.

[65]. V.S. Gugilla, J. Akyurtlu, A. Akyurtlu, I. Blankson, Ind. Eng. Chem. Res. 49 (2010) 8164–8173.

Table Captions

Table 1. Main textural and structural properties of synthesized CeO_2 carrier and Pt/CeO_2 catalysts.

Table 2. Reducibility and reduction species for Pt/CeO_2 catalysts as a function of platinum loading.

Figure Captions

Figure 1. Experimental flame-temperature versus time plots during combustion reaction synthesis.

Figure 2. Global schematic diagram of the experimental setup.

Figure 3. XRD patterns of CeO_2 carrier and Pt/CeO_2 catalysts compared with the reference compound (CeO_2, JPDS 4-593).

Figure 4. TEM images of Pt/CeO_2 catalysts as a function of platinum loading: (a) 0.6-Pt/CeO_2; (b) 1.2-Pt/CeO_2; (c) 2.3-Pt/CeO_2.

Figure 5. H_2-TPR patterns of CeO_2 and Pt/CeO_2 samples.

Figure 6. (a) Scheme of model reactor (quartz tube and furnace) for blank tests; (b) Temperature profiles and carbon formation zone during blank tests (T_C = 400-700°C, S/C = 2); (c) Catalytic bed configuration for n-dodecane SR experiments; (d) temperature gradient profile during n-dodecane SR over 1.2-Pt/CeO_2 catalyst at T_{SET} = 800°C, S/C = 2 and GHSV=24,000 h^{-1}.

Figure 7. Influence of S/C molar ratio on n-dodecane SR over 1.2-Pt/CeO_2 catalyst: n-dodecane conversion, H_2, CO, CO_2 and by-products (CH_4, C_2H_4) concentrations (dry and N_2-free basis) and H_2/CO molar ratio. Equilibrium values are reported as dotted lines. Reaction conditions: T_{SET} = 800°C, S/C = 2.0-3.0, GHSV = 24,000 h^{-1}.

Figure 8. Influence of GHSV on n-dodecane SR over 1.2-Pt/CeO_2 catalyst: n-dodecane conversion, H_2, CO, CO_2 and by-products (CH_4, C_2H_6, C_2H_4) concentrations (dry and N_2-free basis) and H_2/CO molar ratio. Equilibrium values are reported as dotted lines. Reaction conditions: T_{SET} = 800°C, S/C = 2.5, GHSV = 16,000-32,000 h^{-1}.

Figure 9. Influence of platinum loading on n-dodecane SR over Pt/CeO_2 catalysts: n-dodecane conversion, H_2, CO, CO_2 and by-products (CH_4, C_2H_6, C_2H_4) concentrations (dry and N_2-free basis) and H_2/CO molar ratio. Equilibrium values are reported as dotted lines. Reaction conditions: T_{SET} = 800°C, S/C = 2.5, GHSV = 24,000 h^{-1}.

Figure 10. Stability test of n-dodecane SR over (a) 0.6-Pt/CeO_2 catalyst and (b) commercial Rh/ZDC (Rh/Zirconia-Doped-Ceria) catalyst: Product composition (dry and N_2-free basis) and H_2/CO molar ratio. Reaction conditions: T_{SET} = 800°C, S/C = 2.5, GHSV = 16,000 h^{-1}.

Figure 11. Regeneration test of 0.6-Pt/CeO_2 catalyst towards n-dodecane SR: Product composition (dry and N_2-free basis). Reaction conditions: T_{SET} = 800°C, S/C = 1.5, GHSV = 40,000 h^{-1}.

Figure 12. TPO pattern of used (stability test) 0.6- Pt/CeO_2 catalyst.

Figure 13. TEM micrograph of (a) used (stability test) and (b) regenerated 0.6-Pt/CeO_2 catalysts.